Stepwise multipolyubiquitination of p53 by the E6AP-E6 ubiquitin ligase complex

Received for publication, March 10, 2019, and in revised form, August 13, 2019 Published, Papers in Press, September 6, 2019, DOI 10.1074/jbc.RA119.008374

Yuji Masuda[‡§1], Yasushi Saeki[¶], Naoko Arai[¶], Hidehiko Kawai[‖], Iwao Kukimoto[**], Keiji Tanaka[¶], and Chikahide Masutani[‡§]

*From the [‡]Department of Genome Dynamics, Research Institute of Environmental Medicine, Nagoya University, Furo-cho, Chikusa-ku, Nagoya 464-8601, Japan, the [§]Nagoya University Graduate School of Medicine, 65 Tsurumai-cho, Showa-ku, Nagoya 466-8550, Japan, the [¶]Laboratory of Protein Metabolism, Tokyo Metropolitan Institute of Medical Science, 2-1-6 Kamikitazawa, Setagaya-ku, Tokyo 156-8506, Japan, the [‖]Graduate School of Biomedical and Health Sciences, Hiroshima University, 1-2-3 Kasumi, Minami-ku, Hiroshima 734-8553, Japan, and the **Pathogen Genomics Center, National Institute of Infectious Diseases, 4-7-1 Gakuen, Musashi-murayama, Tokyo 208-0011, Japan*

Edited by George N. DeMartino

The human papillomavirus (HPV) oncoprotein E6 specifically binds to E6AP (E6-associated protein), a HECT (homologous to the E6AP C terminus)-type ubiquitin ligase, and directs its ligase activity toward the tumor suppressor p53. To examine the biochemical reaction *in vitro*, we established an efficient reconstitution system for the polyubiquitination of p53 by the E6AP-E6 complex. We demonstrate that E6AP-E6 formed a stable ternary complex with p53, which underwent extensive polyubiquitination when the isolated ternary complex was incubated with E1, E2, and ubiquitin. Mass spectrometry and biochemical analysis of the reaction products identified lysine residues as p53 ubiquitination sites. A p53 mutant with arginine substitutions of its 18 lysine residues was not ubiquitinated. Analysis of additional p53 mutants retaining only one or two intact ubiquitination sites revealed that chain elongation at each of these sites was limited to 5–6-mers. We also determined the size distribution of ubiquitin chains released by *en bloc* cleavage from polyubiquitinated p53 to be 2–6-mers. Taken together, these results strongly suggest that p53 is multipolyubiquitinated with short chains by E6AP-E6. In addition, analysis of growing chains provided strong evidence for step-by-step chain elongation. Thus, we hypothesize that p53 is polyubiquitinated in a stepwise manner through the back-and-forth movement of the C-lobe, and the permissive distance for the movement of the C-lobe restricts the length of the chains in the E6AP-E6-p53 ternary complex. Finally, we show that multipolyubiquitination at different sites provides a signal for proteasomal degradation.

The human papillomavirus (HPV)[2] oncoprotein E6 causes proteasomal degradation of polyubiquitinated p53 by hijacking a cellular HECT (homologous to the E6AP C terminus)-type ubiquitin (Ub) ligase, E6AP (E6-associated protein) (1–5). This biochemical reaction is critical for the oncogenic transformation of HPV-infected cervical cells and is therefore a target of chemical drugs for the treatment of HPV-positive cervical cancer and its prevention in HPV-infected individuals. Improving our understanding of the reaction mechanism underlying the polyubiquitination of p53 by the E6AP-E6 complex could help orientate drug screening and design for the development of effective treatments against HPV-positive cervical cancer.

Among several types of Ub ligases, the mechanism of polyubiquitination mediated by RING (really interesting new gene)-type Ub ligases has been studied extensively. Most RING-type Ub ligases first attach Ub to the target protein, and then transfer a second Ub to the attached Ub moiety; the next Ub is then transferred to the distal Ub moiety, and so on (6). In these reactions, the E2 plays a central role in the determination of linkage and processivity for RING-type E3s (6–8).

By contrast, many questions remain unanswered regarding other types of Ub ligases, especially HECT-type Ub ligases (8). Unlike RING-type Ub ligases, HECT-type Ub ligases are charged with Ub by *trans*-thiolation from E2~Ub (9, 10) and are thought to catalyze all of the following reactions, including substrate selection, priming, and elongation of Ub chains on the substrates and specification of linkage type. Previous studies suggest several potential molecular mechanisms of Ub chain formation by HECT-type Ub ligases (11–22). However, the contribution of each part of the reaction to overall target protein polyubiquitination remains unclear. In this regard, analysis using fully reconstituted systems is necessary to understand how HECT-type Ub ligases execute complex tasks.

The present biochemical study demonstrates that E6AP-E6 forms a ternary complex with p53 and generates multiple Lys[48]-

This work was supported by Japan Society for the Promotion of Science (JSPS) KAKENHI Grants JP15H02818, JP18H03371, and JP16K12594 (to Y. M.); by MEXT KAKENHI Grants JP21000012 and JP26000014 (to K. T.), JP18H05498 and JP18H03993 (to Y. S.), and JP16H01775 (to C. M.); and by the Takeda Science Foundation (to C. M.). The authors declare that they have no conflicts of interest with the contents of this article.
This article was selected as one of our Editors' Picks.
This article contains Table S1 and Figs. S1–S6.

[1] To whom correspondence should be addressed: Dept. of Genome Dynamics, Research Institute of Environmental Medicine, Nagoya University, Furo-cho, Chikusa-ku, Nagoya 464-8601, Japan. Tel.: 81-52-789-3871; Fax: 81-52-789-3890; E-mail: masuda@riem.nagoya-u.ac.jp.

[2] The abbreviations used are: HPV, human papillomavirus; Ub, ubiquitin; HECT, homologous to the E6AP C terminus; RING, really interesting new gene; E6AP, E6-associated protein; USP7, ubiquitin-specific protease 7; AQUA, absolute quantitation; PRM, parallel reaction monitoring; BisTris, 2-[bis(2-hydroxyethyl)amino]-2-(hydroxymethyl)propane-1,3-diol; AMBC, ammonium bicarbonate; ACN, acetonitrile; FA, formic acid.

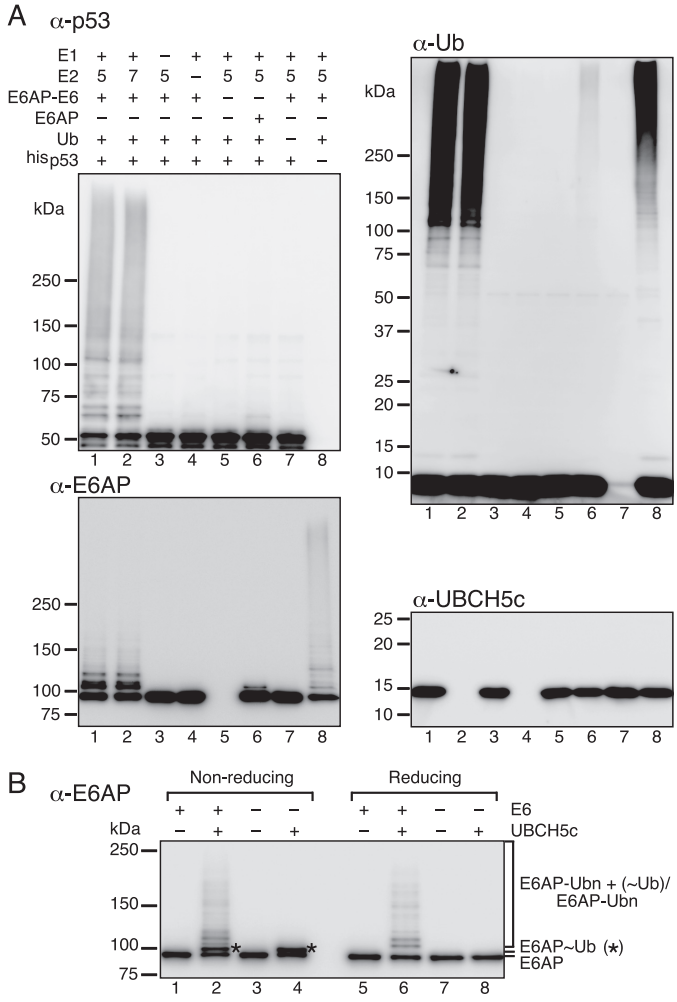

Figure 1. Reconstitution of the polyubiquitination of p53. *A*, reactions were performed under standard conditions, and the products were visualized by Western blotting with the indicated antibodies. For E2s, *5* and *7* indicate UBCH5c and UBCH7, respectively. *B*, formation of the thiol linkage between E6AP and Ub (E6AP~Ub) in the presence or absence of E6. E3-charging assays were performed as described under "Experimental procedures," and the products were analyzed under nonreducing or reducing conditions by Western blotting with anti-E6AP antibody.

linked short poly-Ub chains via stepwise reactions. We hypothesize that p53 is polyubiquitinated in a stepwise manner through the back-and-forth movement of the C-lobe, and the permissive distance for the movement of the C-lobe restricts the length of the chains in the E6AP-E6-p53 ternary complex.

Results

A reconstitution system for the polyubiquitination of p53 by the E6AP-E6 complex in vitro

The biochemical reactions of polyubiquitination by HECT-type Ub ligases were analyzed by establishing a reconstitution system for the polyubiquitination of p53 by E6AP-E6 *in vitro* (Fig. 1 and Fig. S1). Remarkably, co-expression of E6AP and E6 in *Escherichia coli* cells and their subsequent purification as an E6AP-E6 complex yielded a highly active preparation. Standard reactions were performed at 30 °C for 10 min, and the reaction products were detected by Western blotting (Fig. 1). In this system, efficient ubiquitination of ^{his}p53 and self-ubiquitination of E6AP were detected as slower migrating forms in the presence of E1, E2 (UBCH5c or UBCH7), E6, and Ub, as reported previously (Fig. 1*A*) (1, 2, 5, 23–25).

To confirm the formation of thiol linkages between E6AP and Ub (10), assays were performed for 30 s without ^{his}p53 to avoid Ub transfer from E6AP~Ub to ^{his}p53, and the products were analyzed under nonreducing and reducing conditions by Western blotting with anti-E6AP antibody (Fig. 1*B*). The results clearly showed E2-dependent formation of E6AP~Ub in the absence of E6 (*lane 4*), as indicated by the sensitivity of the complex to a reducing agent (*lane 8*). In the presence of E6, many bands larger than E6AP~Ub were detected (*lane 2*). Treatment with the reducing agent resulted in the disappearance of several products; however, some products were still detectable (*lane 6*), suggesting that bands detected under nonreducing conditions were a mixture of self-ubiquitinated E6AP and self-ubiquitinated E6AP with an additional Ub via thiol linkage. These results demonstrated that the reconstitution system efficiently generated E6AP~Ub.

Polyubiquitination in a stable complex consisting of E6AP, E6, and p53

The effect of the concentration of E6AP-E6 on p53 ubiquitination was examined (Fig. 2*A*). Although the amounts of polyubiquitinated products increased in a manner dependent on E6AP-E6 concentration, relatively large products were detectable even in the presence of low E6AP-E6 concentrations. This result suggested that once E6AP-E6 binds to ^{his}p53, it successively transfers many Ub molecules without dissociation (*i.e.* E6AP-E6 might form a stable complex with p53). To examine complex formation, ^{his}E6AP, E6, and p53 were co-produced in *E. coli*. Then ^{his}E6AP was purified in the presence of 1 M NaCl by nickel affinity, and fractionated by gel filtration chromatography to separate ^{his}E6AP-E6 from the ternary complex consisting of ^{his}E6AP, E6, and p53. Each fraction was analyzed again by gel filtration (Fig. 2*B*). The three proteins, ^{his}E6AP, E6, and p53, co-eluted together at 600–700 kDa of apparent molecular mass, which was considerably larger than the mass of ^{his}E6AP-E6 at 170–200 kDa. We analyzed the intensity of each protein component in the peak fractions from the gel images of Fig. 2*B*. The calculated stoichiometries of each subunit in the ^{his}E6AP-E6-p53 and ^{his}E6AP-E6 complexes were close to 1:1:1 and 1:1, respectively (Table 1). The ligase activity of the ternary complex was confirmed by a ubiquitination assay with the additional introduction of E1, UBCH5c, and Ub (Fig. 2*C*). These results suggest that the stable binding of E6AP-E6 to p53 ensures that each p53 molecule is ubiquitinated processively.

Effects of E2 concentration to E6AP trans-thiolation and p53 ubiquitination

Next, the effect of E2 concentration was examined (Fig. 3). The results showed that the concentration of E2 strongly affected the size of the products during a 10-min incubation. Both UBCH5c and UBCH7 supported the ubiquitination of ^{his}p53 at similar concentrations (Fig. 3, *A* and *B*). N-terminal histidine-tagged UBCH5c (^{his}UBCH5c) was inefficient (Fig. 3*C*), as an ~17-fold higher concentration of ^{his}UBCH5c than UBCH5c was required to obtain similar levels of ubiquitination. We also tested two specific mutants of UBCH5c, S22R (desig-

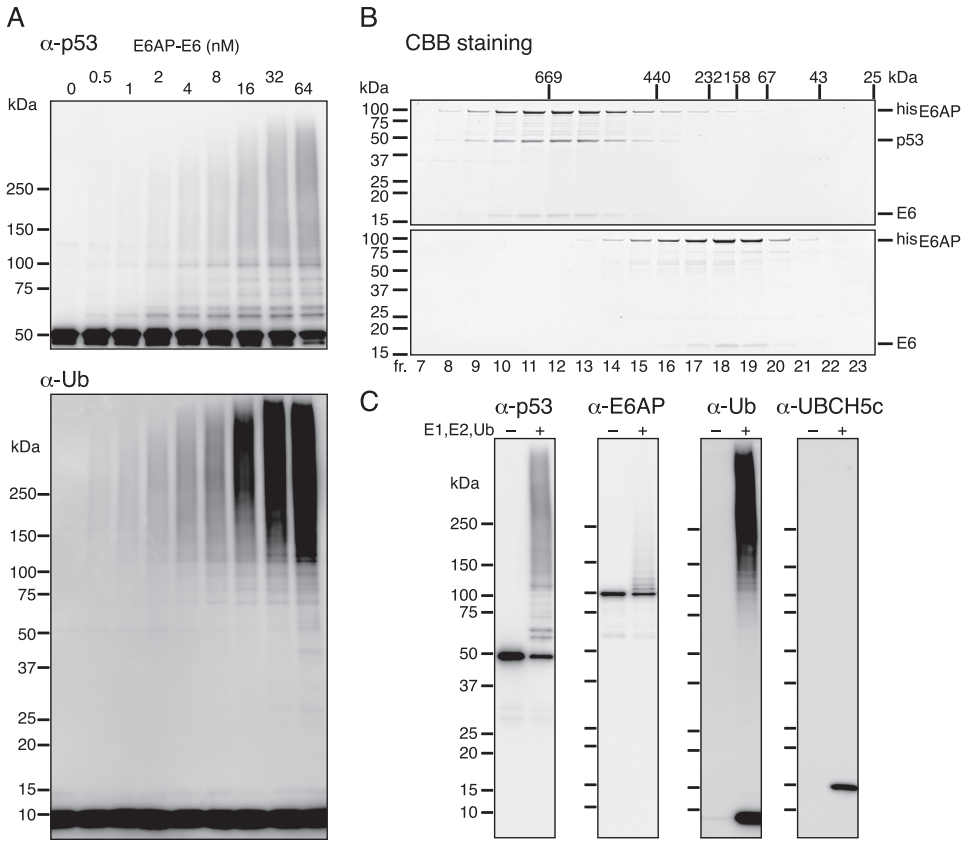

Figure 2. Stable complex formation of E6AP-E6 and p53. *A*, titration of E6AP-E6. Reactions were performed under standard conditions, and the products were visualized by Western blotting with the indicated antibodies. *B*, gel filtration chromatography of ^{his}E6AP-E6-p53 (*top*) and ^{his}E6AP-E6 (*bottom*). Each fraction was analyzed by SDS-PAGE and Coomassie Brilliant Blue staining. *C*, reconstitution of ubiquitination reactions with the purified ternary complex. Reactions were performed under standard conditions with fraction 12 of gel filtration chromatography (*B*, *top*) instead of E6AP-E6 and ^{his}p53. The reaction products were visualized by Western blotting with the indicated antibodies.

Table 1
Stoichiometries of protein components in the ^{his}E6AP-E6-p53 and ^{his}E6AP-E6 complexes

		^{his}E6AP-E6-p53 complex		^{his}E6AP-E6 complex	
Protein	MW[a]	Relative intensity[b]	Stoichiometry[c]	Relative intensity[b]	Stoichiometry[c]
^{his}E6AP	103,000 (1)	1	1	1	1
p53	44,000 (0.43)	0.53	1.2		
E6	18,000 (0.17)	0.20	1.2	0.17	1.0

[a] MW, molecular weight calculated from amino acid sequences. Relative values are shown in parentheses.
[b] The intensities of gel bands were measured from the gel image of Fig. 2*B*, and the relative values are shown.
[c] Stoichiometries were calculated as relative intensities according to the respective relative molecular weight values.

nated as UBCH5c^{SR}), which is deficient in self-assembly of E2∼Ub conjugates and therefore inefficient with RING-type Ub ligases (26, 27), and P61A/F62A (designated as UBCH5c^{2A}), which has reduced affinity for E6AP (28–31). Unlike the RING-type ligases, UBCH5c^{SR} supported p53 ubiquitination by E6AP-E6 (Fig. 3*D*). By contrast, UBCH5c^{2A} showed a clear defect in p53 ubiquitination with ∼2000-fold reduced affinity (Fig. 3*E*). We excluded the possibility that defects in ^{his}UBCH5c and UBCH5c^{2A} were attributed to inefficient E2∼Ub formation catalyzed by E1, because both ^{his}UBCH5c and UBCH5c^{2A} were charged as well as UBCH5c and UBCH5c^{SR} for 30 s (Fig. 3*F*).

Then we analyzed the subsequent reaction step, E6AP *trans*-thiolation (Fig. 3*G*). The reactions were performed for 30 s in the absence of E6 to prevent subsequent Ub transfer to E6AP itself (see Fig. 1*B*). The results showed that UBCH5c and UBCH5c^{SR} supported E6AP∼Ub formation at 50 nM (Fig. 3*G*, *lanes 2* and *3*). By contrast, ^{his}UBCH5c was ineffective at 50 nM but effective at 1600 nM (*lanes 5* and *6*), and UBCH5c^{2A} was apparently defective even at 1600 nM (*lane 4*). These results indicated a positive correlation between the efficiency of p53 ubiquitination and E6AP∼Ub formation, suggesting that *trans*-thiolation is a critical step in determining the rate of p53 ubiquitination.

Kinetics of ubiquitination reactions

The reaction mechanism was further analyzed by examining the time course of the reaction (Fig. 4*A*). The result showed that the size of ubiquitinated ^{his}p53 increased in a time-dependent manner, reaching the maximum level at 30 min. Unanchored

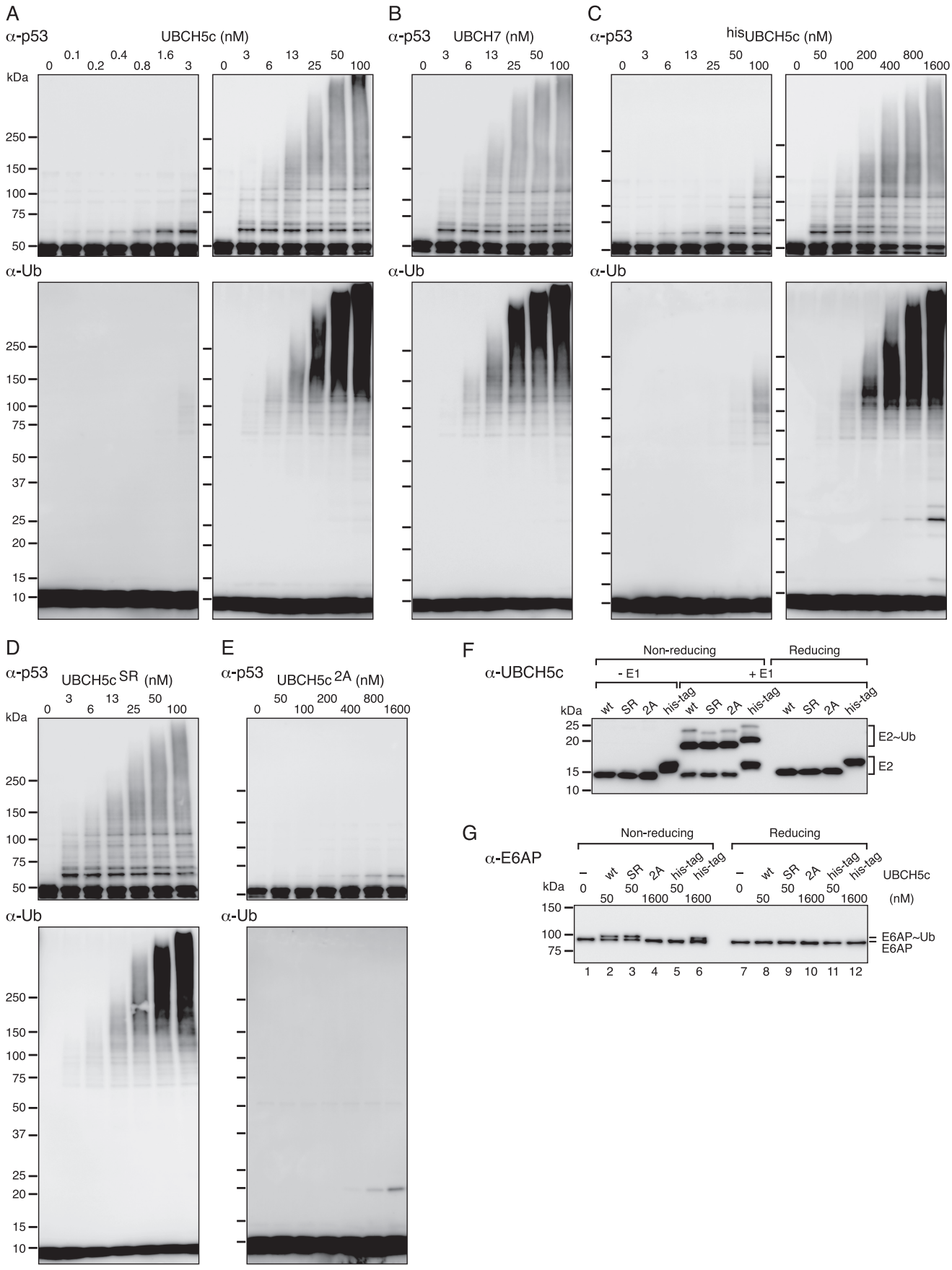
A
α-p53
UBCH5c (nM)
0 0.1 0.2 0.4 0.8 1.6 3
0 3 6 13 25 50 100
kDa
250
150
100
75
50
α-Ub
250
150
100
75
50
37
25
20
15
10
B
α-p53
UBCH7 (nM)
0 3 6 13 25 50 100
α-Ub
C
α-p53
hisUBCH5c (nM)
0 3 6 13 25 50 100
0 50 100 200 400 800 1600
α-Ub
D
α-p53
UBCH5c SR (nM)
0 3 6 13 25 50 100
kDa
250
150
100
75
50
α-Ub
250
150
100
75
50
37
25
20
15
10
E
α-p53
UBCH5c 2A (nM)
0 50 100 200 400 800 1600
α-Ub
F
α-UBCH5c
Non-reducing
Reducing
- E1
+ E1
kDa
wt SR 2A his-tag wt SR 2A his-tag wt SR 2A his-tag
25
20
15
10
E2~Ub
E2
G
α-E6AP
Non-reducing
Reducing
– wt SR 2A his-tag his-tag – wt SR 2A his-tag his-tag
UBCH5c
kDa
0 50 50 50 1600 1600 0 50 50 50 1600 1600
(nM)
150
100
75
E6AP~Ub
E6AP
1 2 3 4 5 6 7 8 9 10 11 12

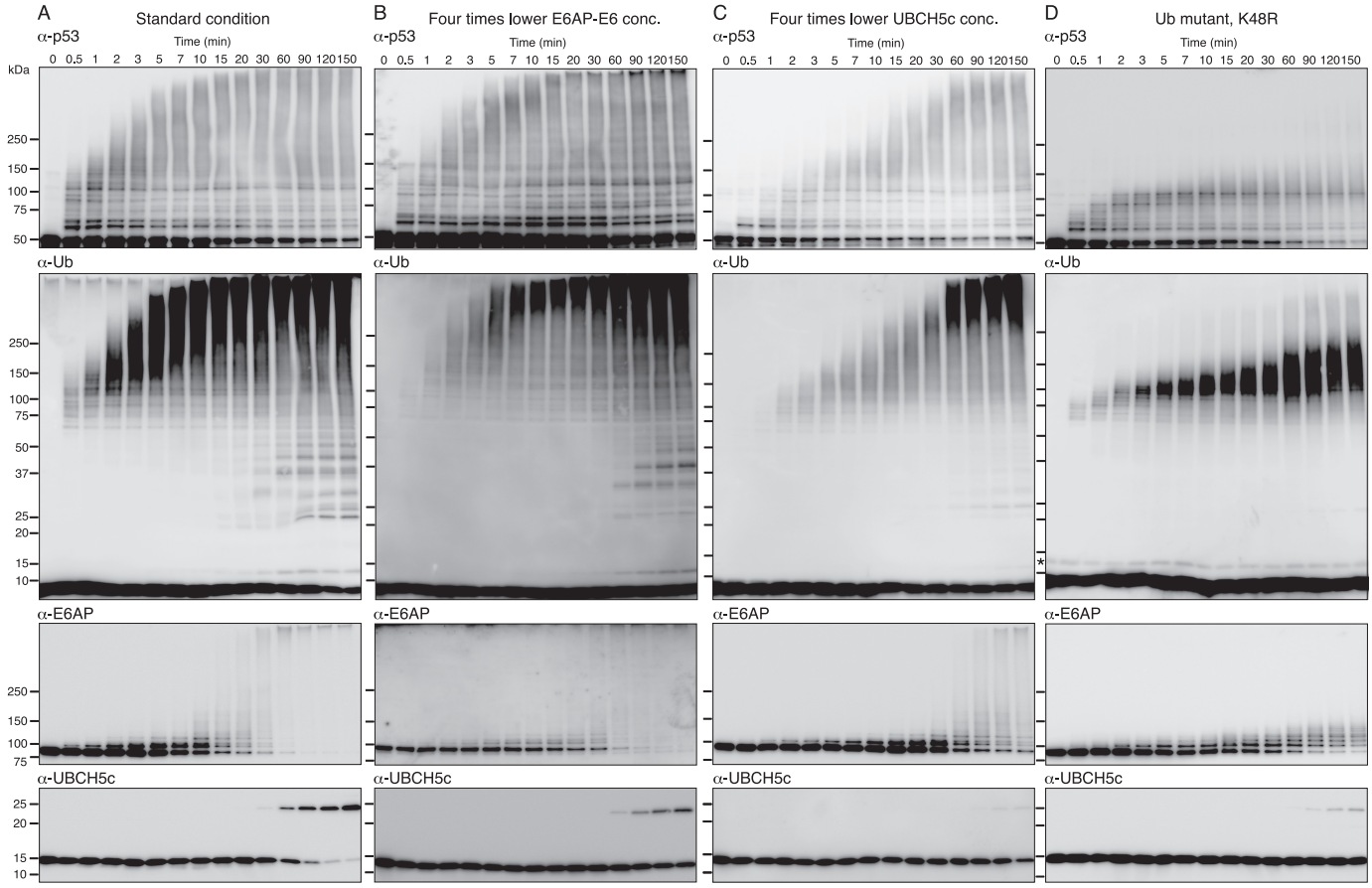

Figure 4. Time courses of the reactions. *A*, the reaction was started in a 250-μl mixture under standard conditions, and 15-μl aliquots were withdrawn at the indicated times. *B*, the reaction was performed as in *A* except for the use of a 4-fold lower E6AP-E6 concentration. *C*, the reaction was performed as in *A* except for the use of a 4-fold lower E2 concentration. *D*, the reaction was performed as in *A* except for the use of the Ub^{K48R} mutant instead of WT Ub. The reaction products were visualized by Western blotting with the indicated antibodies. Note that because of the presence of cross-reacting material (indicated by the *asterisk*) in the commercial Ub^{K48R} preparation (*D*), it was not possible to determine whether or not di-Ub was generated in the reaction.

Ub chains were generated after 15 min and increased considerably after 60 min. Hyperubiquitination of E6AP was initiated at 10 min and reached a maximum level at 60 min. Monoubiquitination of UBCH5c was observed at later time points (Fig. 4*A*). The purified E6AP-E6-p53 complex (Fig. 2*B*) showed similar patterns (Fig. S2*A*).

If polyubiquitination proceeds processively on each ^{his}p53 molecule, a reduced concentration of E6AP should not affect the rate of the chain elongation. To examine this, we analyzed the effect of a lower E6AP-E6 concentration (8 nM, 4-fold lower than the standard concentration) on the time course of polyubiquitination (Fig. 4*B*). As expected, the rates of chain elongation were essentially identical to those of the standard concentration (compare *top panels* of Fig. 4, *A* and *B*). Importantly, large amounts of unmodified ^{his}p53 remained even after a 150-min incubation that resulted in almost all E6AP being self-ubiquitinated (Fig. 4*B*), indicating that ^{his}p53 was present in excess over E6AP-E6. This result supports the notion that each ^{his}p53 molecule undergoes processive polyubiquitination (*i.e.* once an E6AP-E6 molecule binds to a ^{his}p53 molecule, the ^{his}p53 molecule is processively polyubiquitinated by the E6AP-E6 molecule).

By contrast, the E2 concentration strongly affected the rate of ubiquitination of ^{his}p53 (Fig. 3). Thus, the time course was performed under a lower UBCH5c concentration (12.5 nM, 4-fold lower than the standard condition) (Fig. 4*C*). The result showed that the size of ubiquitinated ^{his}p53 increased at a slower rate and reached the maximum level at 60 min; additionally, all other reactions were also delayed. Consistent with the pattern of ^{his}p53-ubiquitination, unanchored Ub chains were generated after 60 min, and hyper-self-ubiquitination of E6AP was now detectable after 60 min. Even after 150 min, E6AP ubiquitination was still partial. Accumulation of unanchored Ub chains and monoubiquitination of UBCH5c were also delayed beyond 150 min (Fig. 4*C*).

It has been established that E6AP specifically generates Lys^{48}-linked Ub chains (11, 12, 32). To confirm this in our reconstitution system, a time course of the reactions was per-

Figure 3. Analysis of the effects of different E2s and their concentrations. *A–E*, titration of E2s. The indicated E2s and mutants were used in the standard reactions. The reaction products were visualized by Western blotting with the indicated antibodies. *F*, E2-charging assay. E2-charging assays were performed as described under "Experimental procedures," and the reaction products were analyzed under nonreducing or reducing conditions by Western blotting with anti-UBCH5c. *G*, E3-charging assay. E3-charging assays were performed in the absence of E6, and the reaction products were analyzed under nonreducing or reducing conditions by Western blotting with anti-E6AP. *his-tag*, ^{his}UBCH5c.

Table 2
Ubiquitin-AQUA/PRM analysis of ubiquitin fragments with GG modifications in lysine residues
Amounts are shown in fmol, and the percentage for each fragment is shown in parentheses.

	Detected fragment[a]										
Ubiquitin	TITLE[b]	Total[c]	Lys^{6}(GG)	Lys^{11}(GG)	Lys^{27}(GG)	Lys^{29}(GG)	Lys^{33}(GG)	Lys^{48}(GG)	Lys^{63}(GG)	M^{1}(GG)	Unmodified[d]
						fmol					
WT	234.4	236.1 (100)	0.04 (<0.1)	1.65 (0.7)	ND[e] (<0.1)	0.0003 (<0.1)	0.07 (<0.1)	115.2 (49.1)	0.08 (<0.1)	ND (<0.1)	25.3 (50.0)
K48R	62.4	65.5 (100)	0.15 (0.2)	3.05 (4.7)	ND (<0.1)	0.002 (<0.1)	0.01 (<0.1)	NA[f]	0.09 (0.1)	ND (<0.1)	37.6 (95.0)

[a] Three independent reaction products were analyzed as described previously (33), and the averages are shown.
[b] The amounts of the TITLE (TITLEVESSDTIDNVLK) fragment were determined as internal controls.
[c] Total ubiquitin levels were assessed as the sum of TITLE, Lys^{11}(GG), and Lys^{27}(GG) fragments. Because the TITLE fragment is between Lys^{11} and Lys^{27}, generation of these fragments is mutually exclusive.
[d] The amounts of unmodified ubiquitin were calculated by subtraction of the amount of total GG-modified fragments from that of total ubiquitin.
[e] ND, not detected.
[f] NA, not applicable because of the mutation.

formed with a Ub mutant, Ub^{K48R} (Fig. 4*D*). In contrast to the reactions performed with WT Ub (Fig. 4*A*), the size of ubiquitinated ^{his}p53 increased to ~110 kDa in the early time points, and then gradually increased to fractions of ~150 kDa together with minor fractions of considerably higher molecular mass (>250 kDa). Such restriction was also observed in the self-ubiquitination of E6AP (Fig. 4*D*). Similar results were obtained with methylated Ub, but the higher-molecular mass species (>250 kDa) were not detectable (Fig. S2*B*). Because Ub is methylated on amino groups and thus unable to form poly-Ub chains, the ubiquitinated products formed by methylated Ub are definitely (multi-)monoubiquitinated forms (33). Thus, the higher-molecular mass species (>250 kDa) detected with Ub^{K48R} (Fig. 4*D*), but not detected with methylated Ub, are most likely polyubiquitinated forms. These results suggested that E6AP predominantly forms Lys^{48} linkages and potentially other linkage(s) inefficiently and that p53 was multiubiquitinated at probably 7–12 sites, as estimated from the size of 110–150 kDa.

Mass spectrometry analysis of Ub chains

The Ub-linkage types in these reactions were also determined by quantitative MS-based analysis called Ub-AQUA (absolute quantitation)/PRM (parallel reaction monitoring) (34). The reaction products (>150 kDa) detected at 10 min for WT Ub and at 30 min for Ub^{K48R} were subjected to Ub-AQUA/PRM. In the WT Ub reaction, most Ub molecules were found in Lys^{48} linkages (49%) or unmodified (50%) (Table 2). Shotgun MS analysis identified 14 lysine residues of p53 as the ubiquitination sites (Fig. 5*A*). Ubiquitination was not detected at four lysine residues. The remaining two lysine residues were not covered by the MS analysis. Some sites were simultaneously ubiquitinated. In the Ub^{K48R} reaction, ~95% was unmodified Ub (Table 2), confirming the predominance of multimonoubiquitination, and a substantial fraction of Lys^{11} linkages (4.7%) was detected (Table 2). The same 14 lysine residues were detected as sites modified with Ub^{K48R} (Fig. 5*B*). These results indicated that the large-molecular weight fractions observed in the Ub^{K48R} reaction contained Lys^{11} linkages.

Analysis of p53 mutants

To confirm the ubiquitination sites identified by MS analysis, the 14 lysine residues of p53 were replaced with arginine residues (Fig. 6*A*). The resultant mutant, $p53^{14KR}$, was then purified as a ternary complex with E6AP-E6 as described for WT p53 above (Fig. S3). The ternary complex was subjected to time course analysis with WT Ub (Fig. 6*B*, *top*). The results demonstrated that $p53^{14KR}$ was still polyubiquitinated. Reactions with Ub^{K48R} revealed at least three additional targets (Fig. 6*B*, *bottom*). To identify these ubiquitination sites, additional mutations were introduced into the $p53^{14KR}$ mutant (Fig. 6*A*). Then ternary complexes were purified (Fig. S3) and subjected to time course analysis with WT Ub or Ub^{K48R}. The $p53^{15KR}$ mutant, which contained an additional K351R mutation (Fig. 6*A*), was ubiquitinated in a manner similar to that of the $p53^{14KR}$ mutant (Fig. 6*C*), confirming the result of MS analysis that Lys^{351} was not a target (Fig. 5). The $p53^{14+2KR}$ mutant, which contained the additional K132R and K139R mutations (Fig. 6*A*), exhibited a slight reduction of ubiquitination with WT Ub, and only two targets were detected with Ub^{K48R} (Fig. 6*D*). Finally, the $p53^{14+4KR}$ mutant, which contained the additional K101R and K120R mutations (Fig. 6*A*), exhibited no apparent ubiquitination (Fig. 6*E*). These results suggested that in addition to the 14 lysine residues detected by MS analysis, four additional lysine residues are potential targets for ubiquitination.

To verify that the ubiquitination sites determined by MS analysis were indeed ubiquitinated, two major ubiquitination sites, Lys^{305} and Lys^{319} (see Fig. 5), were selected and reversed to lysine residues (Fig. 6*A*), and the resulting mutants, $p53^{13(1)+4KR}$ and $p53^{13(2)+4KR}$, were analyzed. The results with Ub^{K48R} confirmed that both mutants had one target for ubiquitination (Fig. 6, *F* and *G*, *bottom panels*). In the reaction with WT Ub, chain elongation was limited to 5–6-mers (Fig. 6, *F* and *G*, *top panels*) despite the fact that these lysine residues are efficient target sites. Then the additional mutant $p53^{12+4KR}$, in which both Lys^{305} and Lys^{319} were reversed to lysine residues (Fig. 6*A*), was analyzed. The results with Ub^{K48R} demonstrated that the two target sites of the $p53^{12+4KR}$ mutant could be simultaneously ubiquitinated, and no preference between the two target sites was observed, because the relative amounts of the two monoubiquitinated forms, distinguishable as two closely migrating doublet bands, were constant over the time course of the reaction (Fig. 6*H*, *bottom*). In the presence of WT Ub, the number of ubiquitin molecules attached to the $p53^{12+4KR}$ mutant was also limited to approximately the sum of those in the single site mutants, $p53^{13(1)+4KR}$ and $p53^{13(2)+4KR}$

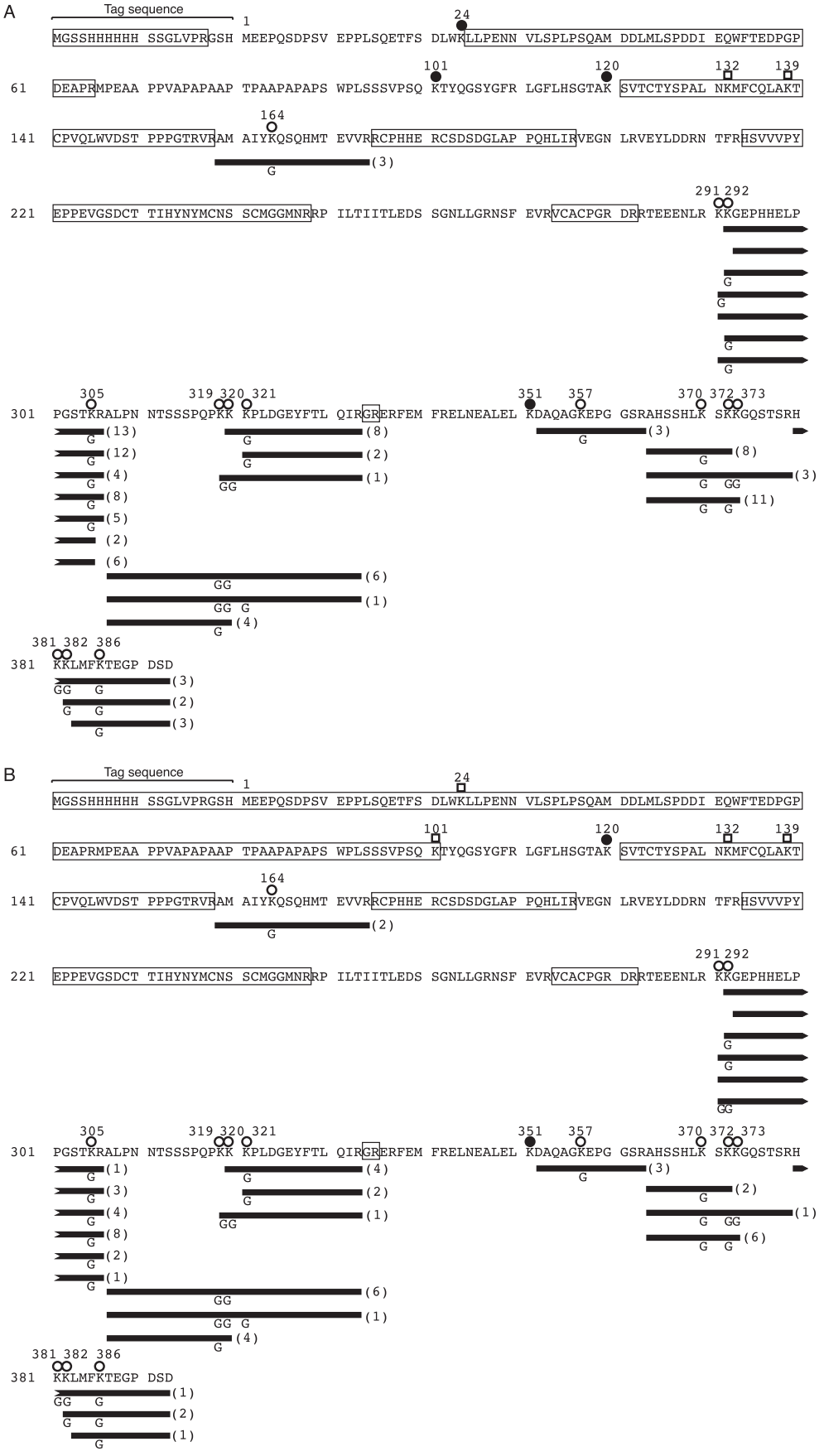
A
Tag sequence
1
24
MGSSHHHHHH SSGLVPRGSH MEEPQSDPSV EPPLSQETFS DLWKLLPENN VLSPLPSQAM DDLMLSPDDI EQWFTEDPGP
101
120
132
139
61 DEAPRMPEAA PPVAPAPAAP TPAAPAPAPS WPLSSSVPSQ KTYQGSYGFR LGFLHSGTAK SVTCTYSPAL NKMFCQLAKT
164
141 CPVQLWVDST PPPGTRVRAM AIYKQSQHMT EVVRRCPHHE RCSDSDGLAP PQHLIRVEGN LRVEYLDDRN TFRHSVVVPY
291 292
221 EPPEVGSDCT TIHYNYMCNS SCMGGMNRRP ILTIITLEDS SGNLLGRNSF EVRVCACPGR DRRTEEENLR KKGEPHHELP
305
319 320 321
351
357
370 372 373
301 PGSTKRALPN NTSSSPQPKK KPLDGEYFTL QIRGRERFEM FRELNEALEL KDAQAGKEPG GSRAHSSHLK SKKGQSTSRH
381 382 386
381 KKLMFKTEGP DSD
B
Tag sequence
1
24
MGSSHHHHHH SSGLVPRGSH MEEPQSDPSV EPPLSQETFS DLWKLLPENN VLSPLPSQAM DDLMLSPDDI EQWFTEDPGP
101
120
132
139
61 DEAPRMPEAA PPVAPAPAAP TPAAPAPAPS WPLSSSVPSQ KTYQGSYGFR LGFLHSGTAK SVTCTYSPAL NKMFCQLAKT
164
141 CPVQLWVDST PPPGTRVRAM AIYKQSQHMT EVVRRCPHHE RCSDSDGLAP PQHLIRVEGN LRVEYLDDRN TFRHSVVVPY
291 292
221 EPPEVGSDCT TIHYNYMCNS SCMGGMNRRP ILTIITLEDS SGNLLGRNSF EVRVCACPGR DRRTEEENLR KKGEPHHELP
305
319 320 321
351
357
370 372 373
301 PGSTKRALPN NTSSSPQPKK KPLDGEYFTL QIRGRERFEM FRELNEALEL KDAQAGKEPG GSRAHSSHLK SKKGQSTSRH
381 382 386
381 KKLMFKTEGP DSD

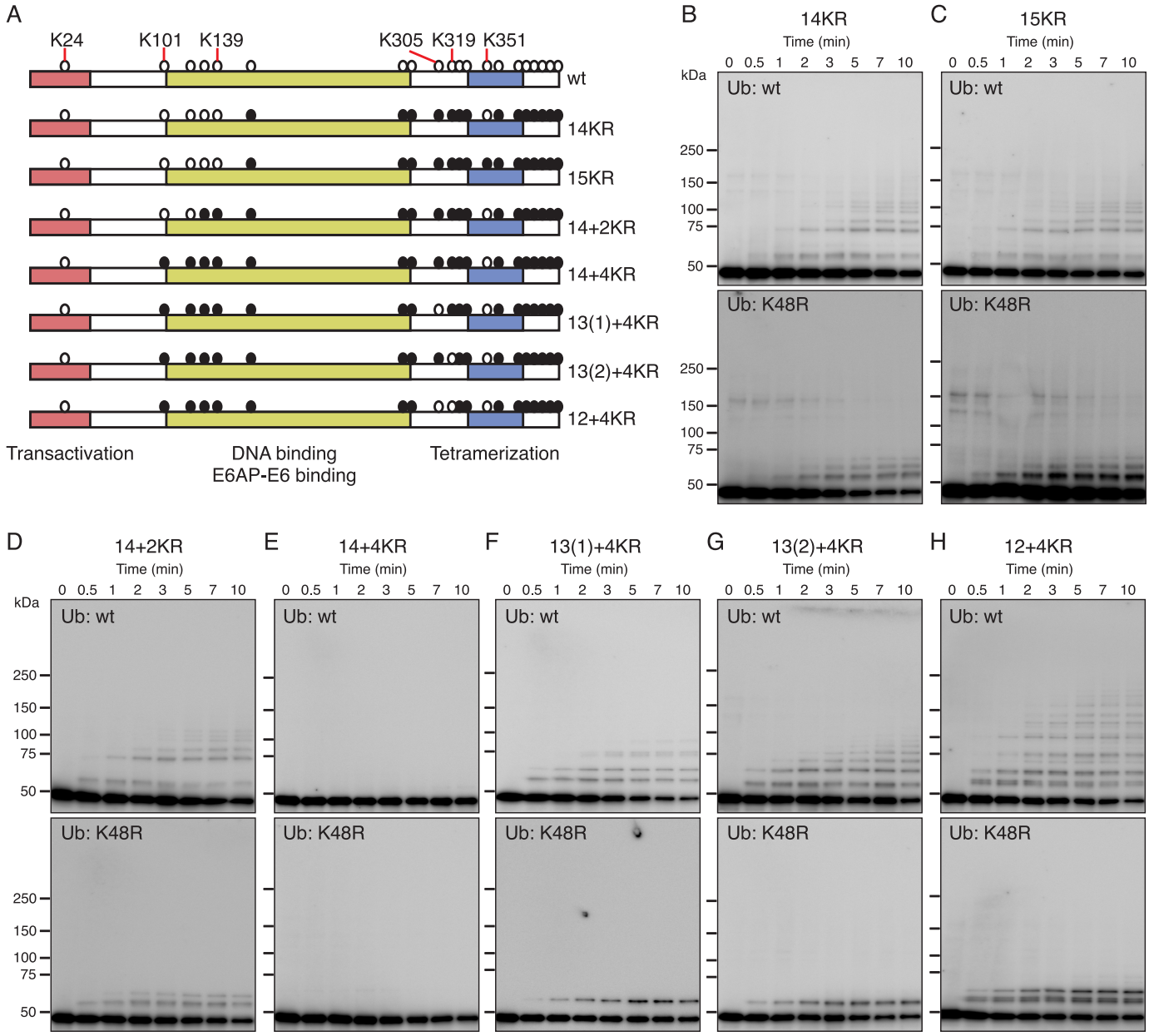

Figure 6. Analysis of p53 mutants. *A*, *schematic representation* of mutation sites in p53. Respective domains are described according to a previous report (52). *Open circles*, positions of lysine residues. *Closed circles*, positions of KR mutations. *B–H*, reconstitution of ubiquitination reactions with the indicated mutant complexes and WT Ub (*top panels*) or Ub^{K48R} (*bottom panels*). Reactions were performed under standard conditions with fraction 12 of gel filtration chromatography (Fig. S3) as shown in Fig. 2*C* and Fig. S2*A*. The reaction products were visualized by Western blotting with anti-p53 antibody.

(Fig. 6*H*, *top*). These results suggested that E6AP-E6 is inefficient at generating long Ub chains, and the high-molecular-weight products generated with WT p53 were a consequence of multiple polyubiquitination with relatively short Ub chains.

Multiple polyubiquitination and stepwise elongation

To demonstrate that WT p53 is multipolyubiquitinated with short chains, we decided to use a deubiquitinating enzyme, USP7, to cleave off and release preferentially substrate-attached Ub chains from ubiquitinated p53. USP7 is ideal for this purpose because it releases unanchored Ub chains from polyubiquitinated substrates through selective digestion of substrate-Ub linkages (35). We focused on Ub chains at early time points of the time course experiments when the size of ubiquitinated ^{his}p53 was constantly increasing (Fig. 4*A*). The reaction products at 3, 5, and 7 min (Fig. 4*A*) were subjected to digestion by ^{his}USP7 for 20–120 min (Fig. 7*A*). Although the released chains were further cleaved upon long incubation with ^{his}USP7, the

Figure 5. Ubiquitination sites in ^{his}p53 determined by shotgun MS analysis. *A* and *B*, reaction products with WT Ub (*A*) or with Ub^{K48R} (*B*) were subjected to MS analysis. Peptide fragments with G-G modifications detected by MS analysis are shown as *black bars* with *numbers* in *parentheses*. The *numbers* indicate the number of fragments detected. The modification sites in the fragments are indicated by *G*. Peptide fragments not covered by MS analysis are enclosed by *open boxes*. Lysine residues marked by *open circles* indicate that ubiquitination was detected, those marked by *closed circles* indicate that ubiquitination was not detected, and those marked by *open squares* indicate that the ubiquitination status is unknown.

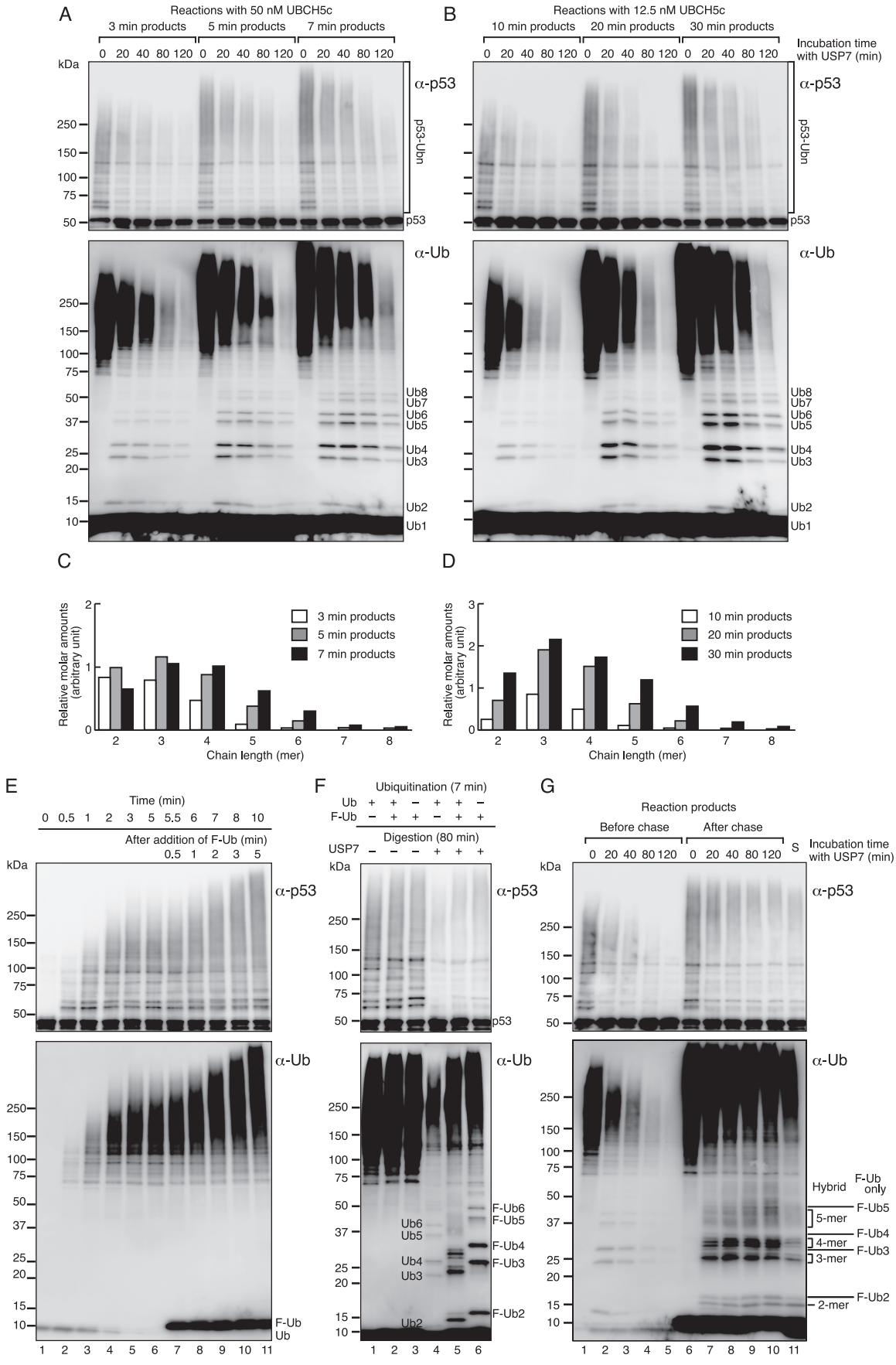
A
Reactions with 50 nM UBCH5c
3 min products
5 min products
7 min products
0 20 40 80 120 0 20 40 80 120 0 20 40 80 120
kDa
α-p53
p53-Ubn
p53
α-Ub
Ub8
Ub7
Ub6
Ub5
Ub4
Ub3
Ub2
Ub1
B
Reactions with 12.5 nM UBCH5c
10 min products
20 min products
30 min products
Incubation time with USP7 (min)
C
Relative molar amounts (arbitrary unit)
3 min products
5 min products
7 min products
Chain length (mer)
D
10 min products
20 min products
30 min products
E
Time (min)
0 0.5 1 2 3 5 5.5 6 7 8 10
After addition of F-Ub (min)
0.5 1 2 3 5
F-Ub
Ub
F
Ubiquitination (7 min)
Ub
F-Ub
Digestion (80 min)
USP7
F-Ub6
F-Ub5
F-Ub4
F-Ub3
F-Ub2
G
Reaction products
Before chase
After chase
S
Hybrid
F-Ub only
5-mer
4-mer
3-mer
2-mer

size distribution of the chains could be addressed at earlier time points. To compare the patterns of the chain distribution, the products after 20-min digestion were quantified (Fig. 7*C*). The result showed that the size of chains increased gradually in a time-dependent manner (Fig. 7*C*), with most chains distributed between dimers and tetramers at 3 min and dimers and pentamers at 5 and 7 min (Fig. 7*C*). We also examined chain lengths in the presence of a lower concentration of UBCH5c (Fig. 7*B*), which resulted in slow chain elongation (Fig. 4*C*). The reaction products at 10, 20, and 30 min (Fig. 4*C*) were subjected to digestion by ^{his}USP7 (Fig. 7*B*), because the size of ubiquitinated p53 was equivalent to that at 3, 5, and 7 min when a high UBCH5c concentration was employed (Fig. 4, compare *A* and *C*). The data obtained after 20 min of digestion were quantified and are shown in Fig. 7*D*. The results were slightly different from those obtained with a high E2 concentration (Fig. 7*C*). The Ub chains showed a peak of trimers at all time points (Fig. 7*D*). The results obtained under both conditions indicated the presence of multipolyubiquitination with relatively short dimer to hexamer chains at the early stages of the reactions. The continuous increase in the total size of ubiquitinated ^{his}p53 during early time points (Fig. 4, *A* and *B*) suggested that this was due to an increase in the number of chains. As a control, we performed the reaction with Ub^{K48R}. Consistent with the results of MS analysis mentioned above (Table 2), Ub ladders were not generated by USP7 treatment when Ub^{K48R} was used in the reactions (Fig. S4*A*), suggesting that p53 mainly underwent multiple monoubiquitination with Ub^{K48R}.

Next, we examined whether the chains were elongated in a stepwise fashion. First, ^{his}p53 was partially ubiquitinated using a low Ub concentration (0.3 μM) for 5 min until the Ub molecules were exhausted (Fig. 7*E* (*lanes 1–6*) and Fig. S4 (*B* and *C*)). Then the reaction was chased by the addition of a large excess of N-terminally FLAG-tagged Ub (^{FLAG}Ub) (Fig. 7*E*, *lanes 7–11*). We assumed that Ub-^{FLAG}Ub hybrid chains would be generated if p53 is polyubiquitinated via stepwise reactions, whereas hybrid chains would not be generated if p53 is polyubiquitinated by *en bloc* reactions only. Whether the Ub-^{FLAG}Ub hybrid chains were generated or not could be determined by making comparisons of the molecular sizes of the released chains. To obtain a standard for Ub-^{FLAG}Ub hybrid chains, polyubiquitination reactions were performed with Ub, ^{FLAG}Ub, or a mixture of both (Fig. 7*F*, *lanes 1–3*), and the chains generated were released by ^{his}USP7 (Fig. 7*F*, *lanes 4–6*). As shown in Fig. 7*F*, hybrid chains with corresponding numbers of ubiquitin molecules (*lane 5*) migrated between corresponding Ub-only chains (*lane 4*) and ^{FLAG}Ub-only chains (*lane 6*) and were clearly separated from each other. Next, polyubiquitinated p53 obtained before and after the addition of ^{FLAG}Ub (Fig. 7*E*) was subjected to ^{his}USP7 digestion, and the sizes of the released chains were compared with those of the standard (Fig. 7*G*). The result revealed multiple bands corresponding to hybrid chains and ^{FLAG}Ub-only chains. Those were distributed from dimer to pentamer and larger chains. This result clearly indicated that respective chains of different lengths were elongated by stepwise reactions.

Table 3
Characteristics of the p53 mutants *in vivo*

p53	E6-dependent degradation[a]	Subcellular distribution[b]	Transactivation[c]
WT	+	Nucleus	+
14KR	+	Nucleus	+
14+4KR	−	Nucleus/cytoplasm	−
13(1)+4KR	−	Nucleus/cytoplasm	−
13(2)+4KR	−	Nucleus/cytoplasm	−
12+4KR	−	Nucleus	−

[a] Data are shown in Fig. 8*A* and Fig. S5.
[b] Data are shown in Fig. S6.
[c] Data are shown in Fig. 8 (*B–D*).

Behavior of p53 mutants in human cells

It is important to determine the characteristics of p53 KR mutants *in vivo* to understand how the fate of p53 and its downstream targets are affected by KR mutations. We therefore examined E6-dependent degradation, subcellular distribution, and transactivation activity of the mutants. N-terminally FLAG-tagged p53 (^{FLAG}p53) KR mutants were transiently expressed in p53-null Saos-2 cells with or without E6 expression. Then protein levels of the p53 mutants after treatment with or without MG132 were analyzed by Western blotting. Expression of ^{FLAG}p53 and endogenous p21 and their subcellular distributions were determined by immunofluorescence staining and subsequent automated fluorescence microscope analysis. Endogenous p21 expression was also analyzed by Western blotting. The results are summarized in Table 3.

As reported previously (36), E6-induced proteasome-dependent degradation of WT ^{FLAG}p53 clearly occurred *in vivo* (Fig. 8*A*). We observed that the ^{FLAG}p53^{14KR} mutant was susceptible to degradation. By contrast, the nonubiquitinated mutant, ^{FLAG}p53^{14+4KR}, was resistant to degradation when it was co-expressed with E6. Interestingly, the other mutants containing one or two efficient ubiquitination sites in their C-terminal regions did not show degradation (Fig. 8*A*). Immunofluorescence staining with two independent anti-p53 antibodies (Fig. S5) confirmed these results.

The subcellular distributions of the mutants are shown in Fig. S6. Two mutants, ^{FLAG}p53^{14KR} and ^{FLAG}p53^{12+4KR}, were predominantly localized to the nucleus, but the other mutants were equally distributed between the nucleus and cytoplasm. The subcellular distributions of the mutants were not affected by E6 co-expression or by MG132 treatment (Fig. S6). This result suggested that the resistance of the ^{FLAG}p53^{12+4KR}

Figure 7. Analysis of the elongation of Ub chains. *A* and *B*, determination of chain length distribution. Reaction products obtained under standard conditions for 3, 5, and 7 min (A) or with 4-fold lower E2 concentrations for 10, 20, and 30 min (*B*) were digested with ^{his}USP7 for the indicated times. *C* and *D*, the signal intensities of the respective chains at 20 min of digestion for *A* and *B* were divided by the number of Ub molecules in the chains, and the calculated values (relative molar amounts of the respective chains) were plotted in *C* and *D*, respectively. *E*, two-step chain elongation reaction. The time course performed with a low amount of Ub (7.5 pmol) was followed by the addition of a large excess of ^{FLAG}Ub (174 pmol). *F*, generation of Ub-^{FLAG}Ub hybrid chains. Reaction products obtained under the standard ubiquitination condition for 7 min with Ub, ^{FLAG}Ub, or a mixture of both (*lanes 1–3*) were digested with USP7 for 80 min (*lanes 4–6*). *G*, evidence of stepwise chain elongation. Reaction products before (5-min incubation with Ub, *lane 6* in *E*) and after the addition of ^{FLAG}Ub (additional 3-min incubation, *lane 10* in *E*) were digested with ^{his}USP7 for the indicated times. The product of the reaction performed with Ub and ^{FLAG}Ub (*lane 5* in *F*) was loaded on the side as a standard (*S*, *lane 11*). *F-Ub*, ^{FLAG}Ub. Reaction products were visualized by Western blotting with the indicated antibodies.

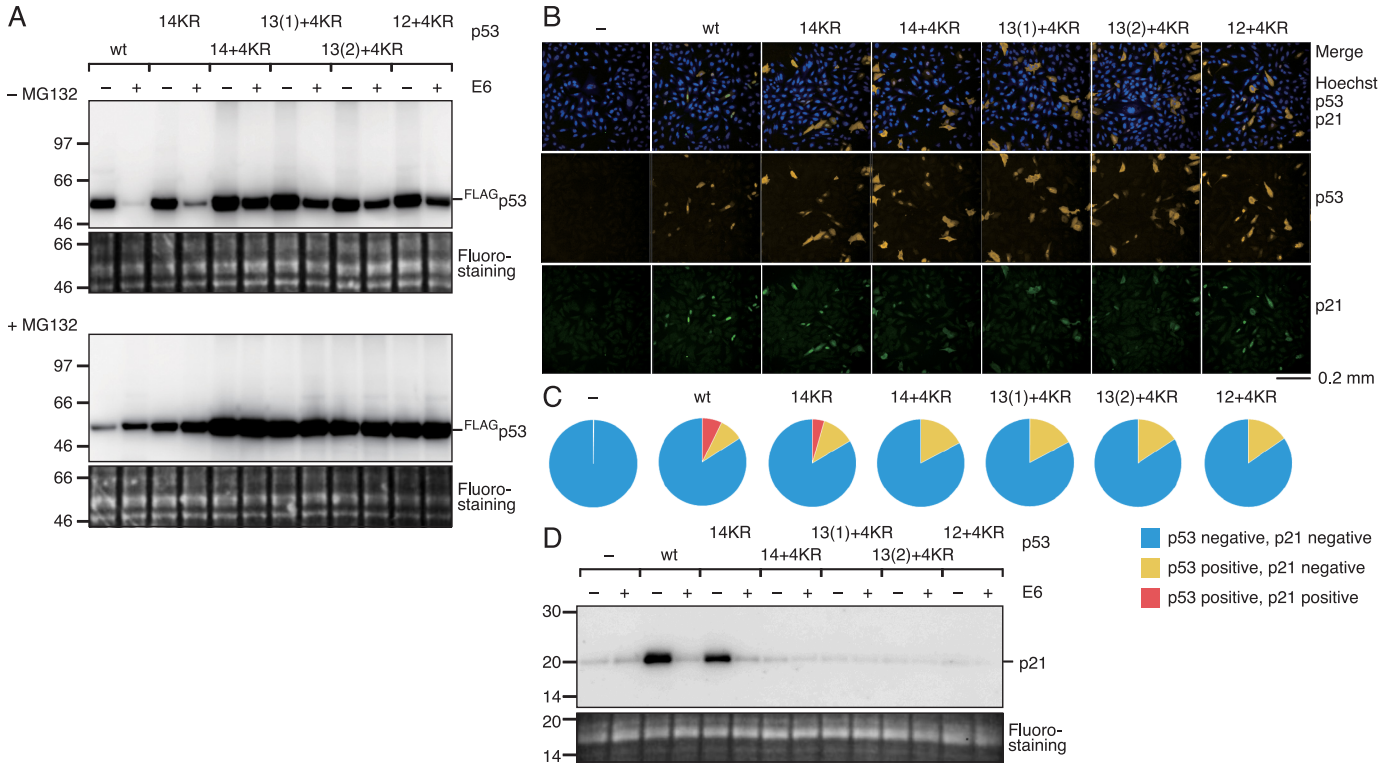

Figure 8. Characterization of p53 mutants in a human p53-null cell line, Saos-2. *A*, the cells were transfected with the indicated ^{FLAG}p53 expression plasmids together with an E6 expression plasmid (+) or the empty vector (−) and then treated with or without MG132 for 6 h, as indicated. ^{FLAG}p53 was visualized by Western blotting with an anti-p53 antibody. An image of the gel loaded with samples stained with the fluorescent dye before transfer to the membrane is shown as a loading control. *B* and *C*, the cells transfected with the indicated plasmids expressing the ^{FLAG}p53 mutants were subjected to automated fluorescence microscope analysis after immunofluorescence staining with an anti-p53 (Alexa Fluor 488–labeled second antibody, *yellow*) and an anti-p21 (Alexa Fluor 488–labeled second antibody, *green*) antibodies, followed by Hoechst 33342 staining. Representative fields acquired from microscope analysis are shown (*B*). Data obtained from more than 1400 cell images under each condition are shown as *pie charts* (*C*). *D*, the cells were transfected with the indicated ^{FLAG}p53 expression plasmids together with an E6 expression plasmid (+) or the empty vector (−). Expression of p21 was visualized by Western blotting with an anti-p21 antibody. An image of fluorostaining as described in *A* is shown as a loading control.

mutant to degradation was not caused by a difference in its subcellular distribution.

The transactivation activities of the mutants were determined by examining their ability to induce endogenous p21 expression. p21 expression was clearly detected in cells transfected with the WT or ^{FLAG}p53^{14KR} expression plasmid, and the p21 signals exclusively co-localized with cells expressing ^{FLAG}p53 (Fig. 8, *B* and *C*). Importantly, co-transfection with the E6 expression plasmid abolished p21 expression (Fig. 8*D*), in parallel with degradation of ^{FLAG}p53^{14KR} or WT ^{FLAG}p53 (Fig. 8*A*). By contrast, none of the other mutants showed transactivation activity (Fig. 8, *B–D*), probably because of defects in their DNA-binding activities caused by additional mutations in the DNA-binding domain of p53 (Fig. 6*A*). Because the transactivation-defective mutants were all resistant to degradation, it is impossible to exclude the possibility that the defect in their DNA-binding activity was somehow related to their increased stability.

Discussion

Specific properties of the E6AP-E6 complex

In the present study, we used recombinant E6AP-E6 purified from *E. coli* simultaneously overproducing both proteins. The binding affinity of E6 to E6AP, which is estimated as 1 nM (37), is high enough to allow its isolation as a stable complex, even after multiple steps of chromatography. The co-purification circumvented the difficulty associated with the purification of the E6 protein itself (38–40) and enabled the generation of highly active E6AP-E6.

We estimated that ^{his}E6AP-E6 had a 1:1 stoichiometry (Table 1). The apparent molecular mass of the ^{his}E6AP-E6 complex analyzed by gel filtration in the presence of 300 mM or 1 M NaCl was 170–200 kDa. This was smaller than the calculated molecular mass of the tetramer, $(E6AP\text{-}E6)_2$, at 244 kDa and larger than that of the heterodimer at 122 kDa. Previously, it was demonstrated that the ligase activity of E6AP is mediated by dynamic intermolecular interactions (37), which are observed even in the presence of E6, because individual E6AP-E6 complexes in a multimer are exchangeable (23, 24). The K_d value of the oligomerization of E6AP has been estimated in the order of magnitude of 10 μM (37). Because of the weak interaction, the multimers are sensitive to protein concentration, pH, and ionic strength (37). Similarly, the K_d value of the dimerization of E6, 290 μM (41), is too high to form a stable complex under the gel filtration conditions used. Taken together with our observation, these reports suggest that the E6AP-E6 complex may have formed a heterodimer under the gel filtration conditions used in the present study and eluted at a higher apparent molecular mass probably because it has a nonglobular shape.

We showed that UBCH5c and UBCH7 similarly supported polyubiquitination of p53 (Fig. 3, *A* and *B*). A mutation at the interface of the interaction with E6AP severely decreased E6AP∼Ub formation (28–31). In addition, the N-terminal extension of UBCH5c interfered with E6AP∼Ub formation, suggesting that the structure of the N terminus is crucial for interaction with E6AP. By contrast, a mutant (UBCH5c^{SR}) that interferes with the E2-Ub interaction (26, 27) did not exhibit any defect. These results indicated that the ability of each E2 to mediate p53-ubiquitination was associated with their capacity for *trans*-thiolation of E6AP, suggesting that the sole function of E2 is the *trans*-thiolation of E6AP. Previously, UBCH5c, UBCH7, and UBCH8 were reported as cognate E2s; however, the relative efficiencies of these E2s differ between reports (28, 42–45). We suggest that these differences could be due to differences in their N-terminal sequences resulting from the addition of tags for purification.

In the reconstitution experiments, polyubiquitination of p53 and E6AP, generation of unanchored Ub chains, and monoubiquitination of UBCH5c were observed; however, these reactions did not occur simultaneously. Analysis of the time course of the reactions revealed that polyubiquitination of p53 mainly occurred during early time points, followed by polyubiquitination of E6AP after the apparent saturation of p53 polyubiquitination. After that, unanchored Ub chains and monoubiquitinated UBCH5c were generated. The observed saturation of polyubiquitination of p53 and E6AP implies that the lengths of poly-Ub chains attached to p53 and E6AP were somehow recognized and restricted (discussed below). The results of the time course experiments indicated that p53 is a better target for ubiquitination than E6AP, suggesting that the thiol-linked Ub at the catalytic cysteine of E6AP is preferentially transferred to p53. This molecular mechanism could explain the inhibition of self-ubiquitination of E6AP by p53 observed previously (23). We also suspect that the generation of unanchored Ub chains and monoubiquitination of UBCH5c are secondary reactions, occurring after the saturation of E6AP self-ubiquitination.

Previously, E6AP was reported to have the potential to form thiol-linked Ub dimers on its catalytic cysteine (12). The authors showed that the reaction was severely limited under low E2 concentrations, such as 50 nM, the concentration employed in the present study (12). Consistently, we were unable to detect the thiol-linked Ub dimers on E6AP and rarely detected free Ub dimers under reducing conditions. Therefore, we suggest that *en bloc* transfer reactions of preformed Ub chains (12) were a minor reaction at relatively low E2 concentrations.

A mechanism to ensure processive polyubiquitination on each p53 molecule

Processive ubiquitination is important for efficient polyubiquitination of target proteins (6). In the present study, we demonstrated that ^{his}E6AP-E6 forms a stable ternary complex with p53 (Fig. 2). The measured stoichiometry of the components in the ternary complex was close to 1:1:1, which is consistent with the reported structure of the E6/E6AP/p53 complex (46). If the ^{his}E6AP-E6 dimer binds to each p53 molecule in a p53 tetramer, the molecular weight would be 660,000, which is close to the apparent molecular mass of 600–700 kDa of the complex eluted from the gel filtration column. In the ternary complex, ^{his}E6AP-E6 could ubiquitinate all p53 molecules in the tetramer (Fig. S2). Time course experiments with different E6AP-E6 concentrations (Fig. 4, *A* and *B*) showed that polyubiquitination was processive on each p53 molecule, strongly suggesting that stable binding of E6AP-E6 to p53 ensures processive p53-ubiquitination on each p53 molecule.

A mechanism for Ub transfer to the distal ends of preformed Ub chains

In the present study, we demonstrated that E6AP-E6 builds multiple poly-Ub chains on p53 through stepwise elongation, as suggested previously (11). We estimated that 7–12 lysine residues in p53 are efficient targets for ubiquitination, and the chain length tended to be restricted to relatively short chains composed of dimers to hexamers. We did not detect any preference for extending existing chains over priming new ones, suggesting that chain elongation was distributive. Recently, French *et al.* (21) reported a mechanism of Ub chain synthesis by another HECT-type Ub ligase, WWP1, which generates Lys^{63}-linked short Ub chains of up to 6-mers via sequential addition; however, the enzyme was inefficient in further chain elongation and instead expanded the chains by adding branched linkages. This is similar to the activity of E6AP in the present study, suggesting that these two ligases share a common catalytic mechanism of ubiquitination. The C-lobe of the HECT domain is connected by a flexible linker to the N-lobe where E2∼Ub binds and has the potential to travel a distance of 40 Å (17, 29). The flexible C-lobe may be able to move around a three-dimensional volume within its reach of at least a radius of 40 Å and potentially transfer Ub to any lysine residues in that area. Therefore, we suggest that the permissive distance for the movement of the C-lobe essentially restricts the length of the chains. The saturation of polyubiquitination revealed by the time course experiments (Fig. 4*A*) may reflect a situation in which all of the available lysine residues within the three-dimensional volume are ubiquitinated.

The properties of E6AP-E6, which transfers Ub onto multiple lysine residues of p53, indicate an intrinsic lower specificity for site selection. By contrast, the transfer of Ub to the Ub moiety attached to p53 was strictly specific to the Lys^{48} residue. These observations raise the question of how the Lys^{48} residue is specified and/or other lysine residues in Ub are rejected during chain elongation reactions. Lys^{48} linkage formation could be determined by the specific interaction between the C-lobe of E6AP and the acceptor Ub (11, 19). Further study is needed to elucidate the molecular mechanism underlying linkage determination.

Implications of polyubiquitination at multiple sites for p53 degradation

We found that one of the p53 KR mutants, p53^{14KR}, was susceptible to E6-dependent degradation (Fig. 8*A*), suggesting that polyubiquitination of p53^{14KR} at not more than four lysine residues (Lys^{101}, Lys^{120}, Lys^{132}, and Lys^{139}) provides an adequate signal for efficient proteasomal degradation. By contrast, polyubiquitination of the p53^{12+4KR} mutant at two lysine resi-

dues (Lys^{305} and Lys^{319}) did not induce degradation (Fig. 8*A*), suggesting that polyubiquitination at those lysine residues is not sufficient for proteasomal degradation. These results are consistent with a model derived from single-molecule kinetic analysis of model substrates by the proteasome *in vitro*, in which multiple ubiquitination with short ubiquitin chains (diubiquitin is sufficient) provided a configuration of chains that efficiently directed the substrate into the translocation channel of the proteasome (47). Although we do not have direct evidence for multipolyubiquitination of p53 *in vivo*, the results suggest that the combination of polyubiquitin chains at the four sites of $p53^{14KR}$, but not at the two sites of $p53^{12+4KR}$, provided the configuration for degradation by the proteasome.

So far, we have no evidence to suggest a defined order of multipolyubiquitination. Rather, the results suggest that selection of different lysine residues during priming and each step of elongation is random, at least *in vitro*. Therefore, we suggest that random ubiquitination by HECT-type Ub ligases occurs at multiple sites with short Ub chains and that the resulting configuration of Ub chains is particularly suited for the initiation of degradation of p53 (47). Further analysis with more p53 KR mutants with different combinations of ubiquitination sites may provide a more complete picture of the optimal combination of ubiquitination sites required for proteasomal degradation.

Experimental procedures

Proteins

The Ub mutant, Ub^{K48R}, and methylated Ub were purchased from Boston Biochem (UM-K48R and U-501, respectively). The expression plasmids for intact E6AP (isoform II), UBCH5c, and UBCH7 were constructed in pET-20b(+). The genes encoding E6 of human papillomavirus type 16 (48) and p53 were respectively cloned into pACYCDuet-1 (Novagen) and pGBM2 with a T7 promoter, as described previously (49). For N-terminally histidine-tagged proteins, the genes encoding p53 and UBCH5c were cloned into pET-15b, and E6AP was cloned into pET-28a(+).

Recombinant human proteins were produced in *E. coli* BL21 (DE3) at 15 °C by the addition of isopropyl β-$_D$-1-thiogalactopyranoside at 0.2 mM, and purified by chromatography at 4 °C using columns from GE Healthcare. Purification of the respective mutants was performed as described for the WT proteins unless otherwise indicated. E1, Ub, and ^{his}USP7 were purified as described previously (35, 50). ^{FLAG}Ub was expressed in BL21 (DE3) harboring pET20-FLAG-Ub, a pET20-Ub derivative (50), and purified, after ammonium sulfate fractionation of cell lysates, by HiTrap Phenyl FF (high sub), HiTrap Heparin HP, and HiTrap Q FF chromatography. E6AP was expressed in BL21 (DE3) harboring pET20-E6AP and purified using the columns HiTrap SP HP, HiTrap Heparin HP, HiTrap Q HP, and Superdex 200. The E6AP-E6 complex was co-expressed in BL21 (DE3) harboring pET20-E6AP and pACYC-E6 and purified as described for E6AP. The ^{his}E6AP-E6 complex was co-expressed in BL21 (DE3) harboring pET28-hisE6AP and pACYC-E6 and purified using the columns Ni^{2+}-charged HiTrap Chelating HP and Superdex 200. UBCH5c was expressed in BL21 (DE3) harboring pET20-UBCH5c and purified using the columns HiTrap DEAE FF, HiTrap SP FF, HiTrap Heparin HP, and Superdex 200. UBCH7 was expressed in BL21 (DE3) harboring pET20-UBCH7 and purified as described for UBCH5c. ^{his}UBCH5c was expressed in BL21 (DE3) harboring pET15-hisUBCH5c and purified using the columns Ni^{2+}-charged HiTrap Chelating HP, HiTrap SP XL, and Superdex 200. ^{his}p53 was expressed in BL21 (DE3) harboring pET15-hisp53 and purified using Ni^{2+}-charged HiTrap Chelating HP. A ternary complex of ^{his}E6AP, E6, and p53 was expressed in BL21 (DE3) harboring pET28-hisE6AP, pACYC-E6, and pGBM-p53 and purified using the columns Ni^{2+}-charged HiTrap Chelating HP and Superdex 200. The intensities of the respective protein bands were measured by ImageJ software from a gel image obtained by scanning the wet SDS-polyacrylamide gel stained by Coomassie Brilliant Blue. Protein concentrations were determined using the Bio-Rad protein assay with BSA (Bio-Rad) as the standard.

Ubiquitination assays

The standard reaction mixture (25 μl) contained 20 mM HEPES-NaOH (pH 7.5), 50 mM NaCl, 0.02 mg/ml BSA, 1 mM DTT, 5 mM $MgCl_2$, 1 mM ATP, ^{his}p53 (1 pmol as a tetramer), E1 (0.85 pmol), UBCH5c (1.25 pmol), E3 (0.8 pmol), and Ub (174 pmol). Reaction mixtures were prepared on ice and then incubated at 30 °C for 10 min unless otherwise indicated. The reactions were terminated by the addition of SDS-sample buffer.

Western blotting

Products were analyzed by Western blotting. Anti-E6AP (GeneTex, UBE3A antibody, GTX10487 or in-house-generated anti-E6AP serum raised in rabbits against the peptide KKG-PRVDPLETELGVKTLDC), anti-p53 (Calbiochem, anti-p53 (Ab-6) mouse mAb (DO-1), OP43), anti-UBCH5c (Ab Frontier, anti-UBE2D3 (4C1-1E3), LF-MA10362), anti-Ub (Santa Cruz Biotechnology, Inc., Ub (P4D1), sc-8017), and anti-FLAG (Sigma-Aldrich, monoclonal anti-FLAG M2, F 1804) were used. Signals were detected with a Chemi-Lumi One L kit (Nacalai Tesque, 07880-70) using ImageQuant™ LAS 4000 Mini Biomolecular Imager (GE Healthcare) and analyzed using ImageJ 1.48v software (National Institutes of Health). When "reducing" or unless otherwise indicated, the samples were treated with SDS-sample buffer containing 280 mM β-mercaptoethanol or 100 mM DTT. When the samples were not treated with any reducing agent, they were described as "nonreducing."

E2-charging assays

The reaction mixture (25 μl) containing 20 mM HEPES-NaOH (pH 7.5), 50 mM NaCl, 0.02 mg/ml BSA, 1 mM DTT, 5 mM $MgCl_2$, 1 mM ATP, E2 (10 pmol), and Ub (174 pmol) was preincubated at 30 °C for 1 min. Reactions were started by the addition of E1 (0.85 pmol) and terminated by the addition of SDS-sample buffer with or without reducing agents after a 30-s incubation at 30 °C.

E3-charging assays

The reaction mixture (25 μl) containing 20 mM HEPES-NaOH (pH 7.5), 50 mM NaCl, 0.02 mg/ml BSA, 1 mM DTT, 5

mM $MgCl_2$, 1 mM ATP, E1 (0.85 pmol), E2 (1.25 pmol), and Ub (174 pmol) was preincubated at 30 °C for 1 min. Reactions were started by the addition of E3 (0.8 pmol) and terminated by the addition of SDS-sample buffer with or without reducing agents after a 30-s incubation at 30 °C.

Analysis of polyubiquitin chains by digestion with USP7

For digestion of the reaction products with ^{his}USP7, DTT was introduced at 5 mM after the ubiquitination reactions were terminated by the addition of EDTA at 20 mM. Digestion was performed with 500 ng of ^{his}USP7 per 10 μl of reaction mixture at 30 °C for the indicated times.

Ub-AQUA/PRM

MS/MS-based quantification of Ub peptides by PRM was performed as described previously (34). To minimize nonspecific adsorption of peptides, Protein LoBind tubes (Eppendorf) and ProteoSave MS vials (AMR Inc.) were used. Ubiquitination reactions were performed under standard conditions except for the absence of BSA for 10 min with the WT or for 30 min with Ub^{K48R}. The reaction products were separated by 4–12% NuPAGE BisTris gels (Life Technologies) with a short run (3 cm). The gels were stained with Bio-Safe Coomassie Stain (Bio-Rad). After the gels were extensively washed with Milli-Q water (Millipore), the gel region above 150 kDa was excised, cut into 1-mm^3 pieces, destained for 1 h with 1 ml of 50 mM ammonium bicarbonate (AMBC), 30% acetonitrile (ACN), with agitation, and then further washed for 1 h with 1 ml of 50 mM AMBC, 50% ACN. Finally, a 100% ACN wash was performed to ensure complete gel dehydration. Trypsin solution (Promega, 20 ng/μl in 50 mM AMBC, 5% ACN) was subsequently added to the gel pieces at approximately equivalent volumes followed by incubation on ice for 30 min. After the addition of another small volume of trypsin solution, the gel samples were incubated at 37 °C overnight. Digests were extracted by the addition of 100 μl of 50% ACN, 0.1% TFA for 1 h with shaking. The peptides were recovered into fresh Eppendorf tubes, and an additional extraction step was performed with 70% ACN, 0.1% TFA for 30 min. The extracted peptides were concentrated using a SpeedVac, added to the AQUA peptides (Table S1), and oxidized with 0.05% H_2O_2, 0.1% TFA for 12 h at 4 °C. The peptides were analyzed in targeted MS/MS mode on a Q Exactive mass spectrometer coupled with an EASY-nLC 1000 liquid chromatograph and nanoelectrospray ion source (Thermo Scientific). The mobile phases were 0.1% formic acid (FA) in water (solvent A) and 0.1% FA in 100% ACN (solvent B). Peptides were directly loaded onto a C18 analytical column (ReproSil-Pur 3 μm, 75-μm inner diameter and 12-cm length, Nikkyo Technos) and separated using a 90-min three-step gradient (0–10% solvent B for 5 min, 10–30% for 70 min and 30–80% for 5 min) at a constant flow rate of 300 nl/min. Ionization was performed with a liquid junction voltage of 1.8 kV and capillary temperature of 250 °C. The Q Exactive was operated by the Xcalibur software in the target MS/MS mode, with an Orbitrap resolution of 70,000 at m/z 200, target automatic gain control values of 1×10^6, maximum ion fill times of 200 ms, an isolation window of 2.0 m/z, and fragmentation by HCD with normalized collision energies of 28. Raw data were processed using PinPoint software version 1.3 (Thermo Scientific).

Shotgun MS analysis

The tryptic digests described above were also subjected to shotgun MS analysis. Separation and elution from the column were achieved using a 40-min two-step gradient (0–35% solvent B for 35 min and 35–100% for 5 min) at a constant flow rate of 300 nl/min. The Q Exactive was operated in the data-dependent MS/MS mode, using Xcalibur software, with survey scans acquired at a resolution of 70,000 at m/z 200. The top 10 most abundant isotope patterns with charge 2–5 were selected from the survey scans with an isolation window of 2.0 m/z and fragmented by HCD with normalized collision energies of 28. The maximum ion injection times were 60 ms for both survey and MS/MS scans, and the automatic gain control values were set to 3×10^6 and 5×10^5 for the survey and MS/MS scans, respectively. Ions selected for MS/MS were dynamically excluded for 10 s. Proteome Discoverer software (version 1.3, Thermo Scientific) was used to generate peak lists. The MS/MS spectra were searched against a Swiss-Prot database (version 2012_10 of the UniProtKB/Swiss-Prot protein database) supplemented with the amino acid sequences of recombinant proteins using the SEQUEST search engine. The precursor and fragment mass tolerances were set to 10 ppm and 20 milli mass units, respectively. Methionine oxidation, deamidation, and diglycine modification of lysine and cysteine side chains were set as variable modifications for database searching. Peptide identification was filtered at a 1% false discovery rate, and high-confidence peptides are shown in Fig. 5.

Cell culture, transfection, and Western blotting

Human osteoblast-like Saos-2 cells were maintained in minimum essential medium Eagle, α modification (Sigma-Aldrich) supplemented with 10% fetal bovine serum and L-glutamine. Plasmid DNAs (pcDNA-FLAG-tagged-p53-WT (51) or -mutant plasmid DNAs with either pcAGGS-empty or -E6 plasmid DNAs) were introduced into Saos-2 cells using LipofectAMINE3000 (Thermo Fisher Scientific) following the manufacturer's instructions. Briefly, cells were plated in 24-well plates 18 h before transfection and then incubated with the plasmid DNAs/LipofectAMINE3000 mixture (0.1 μg of pcDNA-FLAG-p53s and 0.5 μg of pcAGGS-E6 or empty vector per well) for 6 h, after which the medium was replaced with fresh medium, and the cells were incubated for another 24 h. The proteasome inhibitor MG132 (final concentration 7.5 μM) (Thermo Fisher Scientific) was added to the wells 6 h before harvesting the cells. Western blotting was performed using EzLabel FluoroNeo (ATTO), EzRun (ATTO), and EzFastBlot (ATTO) following the manufacturer's instructions. Briefly, whole-cell lysates were prepared with the fluorescent labeling reagent and electrophoresed in a 5–20% gradient gel (e-PAGEL, ATTO). Following transfer, membranes were subjected to Western blotting using an anti-p53 antibody (DO-1, 1:1000, Thermo Fisher Scientific) or an anti-p21 antibody (6B6, 1:1000, BD Pharmingen), followed by a goat anti-mouse IgG (H+L) secondary antibody, horseradish peroxidase (1:1000, Thermo Fisher Scientific). The chemiluminescent signals

were detected by a Luminata Forte (Thermo Fisher Scientific) and ImageQuant LAS 4000 mini (GE Healthcare).

Immunostaining and automated fluorescence microscope analysis

Plasmid DNAs were introduced into Saos-2 cells using LipofectAMINE3000 as described above. Briefly, cells were plated in 384-well plates 18 h before transfection and then incubated with plasmid DNAs/LipofectAMINE3000 mixture (0.02 μg of pcDNA-FLAG-p53s and 0.1 μg of pcAGGS-E6 or empty vector per well) for 6 h, after which the medium was replaced with fresh medium, and the cells were incubated for another 24 h. The proteasome inhibitor MG132 (final concentration 7.5 μM) (Thermo Fisher Scientific) was added to the wells 6 h before 4% paraformaldehyde (Nacalai Tesque) fixation. After Triton X-100 (0.5%) treatment, double immunofluorescence staining was performed using an anti-p53 antibody (FL-393, 1:500, Santa Cruz Biotechnology), an anti-p53 antibody (DO-1, 1:1000, Thermo Fisher Scientific), and an anti-p21 antibody (6B6, 1:1000, BD Pharmingen), followed by a rabbit IgG(H+L) secondary antibody (Alexa Fluor 555, 1:1000, Thermo Fisher Scientific) or a mouse IgG(H+L) cross-adsorbed secondary antibody (Alexa Fluor 488, 1:1000, Thermo Fisher Scientific). After Hoechst 33342 (10 μg/ml, Thermo Fisher Scientific) staining, confocal fluorescent Image stacks (five planes, 2.5-μm intervals) were acquired using Opera Phenix (PerkinElmer Life Sciences) with a ×20 water immersion objective lens. All stacked images were analyzed using the Harmony High Content Imaging and Analysis Software (PerkinElmer Life Sciences), and the area of each nucleus/cytoplasm/cell from the signal of Hoechst 33342 staining and the intensity of each fluorescence per area was calculated. The histo-box plots (Fig. S5) and scatter plots (Fig. S6) were generated using SpotFire (TIBCO).

Author contributions—Y. M. and C. M. conceived the project. Y. M. designed and performed biochemical analyses. Y. S., N. A., and K. T. performed MS analyses. H. K. designed and performed *in vivo* analyses. I. K. contributed materials. Y. M., Y. S., H. K., K. T., and C. M. wrote the paper.

Acknowledgments—We thank Dr. Fumiaki Ohtake (Laboratory of Protein Metabolism, Tokyo Metropolitan Institute of Medical Science, Tokyo, Japan) for comments on the manuscript. We are grateful to Yukiko Takeuchi for laboratory assistance. Automated fluorescence microscope analysis was supported by the Program of the Network-type Joint Usage/Research Center for Radiation Disaster Medical Science, Hiroshima University.

References

1. Scheffner, M., Huibregtse, J. M., Vierstra, R. D., and Howley, P. M. (1993) The HPV-16 E6 and E6-AP complex functions as a ubiquitin-protein ligase in the ubiquitination of p53. *Cell* **75,** 495–505 CrossRef Medline
2. Shkedy, D., Gonen, H., Bercovich, B., and Ciechanover, A. (1994) Complete reconstitution of conjugation and subsequent degradation of the tumor suppressor protein p53 by purified components of the ubiquitin proteolytic system. *FEBS Lett.* **348,** 126–130 CrossRef Medline
3. Huibregtse, J. M., Scheffner, M., and Howley, P. M. (1991) A cellular protein mediates association of p53 with the E6 oncoprotein of human papillomavirus types 16 or 18. *EMBO J.* **10,** 4129–4135 CrossRef Medline
4. Scheffner, M., Werness, B. A., Huibregtse, J. M., Levine, A. J., and Howley, P. M. (1990) The E6 oncoprotein encoded by human papillomavirus types 16 and 18 promotes the degradation of p53. *Cell* **63,** 1129–1136 CrossRef Medline
5. Huibregtse, J. M., Scheffner, M., and Howley, P. M. (1993) Localization of the E6-AP regions that direct human papillomavirus E6 binding, association with p53, and ubiquitination of associated proteins. *Mol. Cell. Biol.* **13,** 4918–4927 CrossRef Medline
6. Ye, Y., and Rape, M. (2009) Building ubiquitin chains: E2 enzymes at work. *Nat. Rev. Mol. Cell Biol.* **10,** 755–764 CrossRef Medline
7. Stewart, M. D., Ritterhoff, T., Klevit, R. E., and Brzovic, P. S. (2016) E2 enzymes: more than just middle men. *Cell Res.* **26,** 423–440 CrossRef Medline
8. Komander, D., and Rape, M. (2012) The ubiquitin code. *Annu. Rev. Biochem.* **81,** 203–229 CrossRef Medline
9. Huibregtse, J. M., Scheffner, M., Beaudenon, S., and Howley, P. M. (1995) A family of proteins structurally and functionally related to the E6-AP ubiquitin-protein ligase. *Proc. Natl. Acad. Sci. U.S.A.* **92,** 2563–2567 CrossRef Medline
10. Scheffner, M., Nuber, U., and Huibregtse, J. M. (1995) Protein ubiquitination involving an E1-E2-E3 enzyme ubiquitin thioester cascade. *Nature* **373,** 81–83 CrossRef Medline
11. Kim, H. C., and Huibregtse, J. M. (2009) Polyubiquitination by HECT E3s and the determinants of chain type specificity. *Mol. Cell. Biol.* **29,** 3307–3318 CrossRef Medline
12. Wang, M., and Pickart, C. M. (2005) Different HECT domain ubiquitin ligases employ distinct mechanisms of polyubiquitin chain synthesis. *EMBO J.* **24,** 4324–4333 CrossRef Medline
13. French, M. E., Kretzmann, B. R., and Hicke, L. (2009) Regulation of the RSP5 ubiquitin ligase by an intrinsic ubiquitin-binding site. *J. Biol. Chem.* **284,** 12071–12079 CrossRef Medline
14. Kamadurai, H. B., Qiu, Y., Deng, A., Harrison, J. S., Macdonald, C., Actis, M., Rodrigues, P., Miller, D. J., Souphron, J., Lewis, S. M., Kurinov, I., Fujii, N., Hammel, M., Piper, R., Kuhlman, B., and Schulman, B. A. (2013) Mechanism of ubiquitin ligation and lysine prioritization by a HECT E3. *eLife* **2,** e00828 CrossRef Medline
15. Kim, H. C., Steffen, A. M., Oldham, M. L., Chen, J., and Huibregtse, J. M. (2011) Structure and function of a HECT domain ubiquitin-binding site. *EMBO Rep.* **12,** 334–341 CrossRef Medline
16. Wang, M., Cheng, D., Peng, J., and Pickart, C. M. (2006) Molecular determinants of polyubiquitin linkage selection by an HECT ubiquitin ligase. *EMBO J.* **25,** 1710–1719 CrossRef Medline
17. Verdecia, M. A., Joazeiro, C. A., Wells, N. J., Ferrer, J. L., Bowman, M. E., Hunter, T., and Noel, J. P. (2003) Conformational flexibility underlies ubiquitin ligation mediated by the WWP1 HECT domain E3 ligase. *Mol. Cell* **11,** 249–259 CrossRef Medline
18. Maspero, E., Mari, S., Valentini, E., Musacchio, A., Fish, A., Pasqualato, S., and Polo, S. (2011) Structure of the HECT:ubiquitin complex and its role in ubiquitin chain elongation. *EMBO Rep.* **12,** 342–349 CrossRef Medline
19. Maspero, E., Valentini, E., Mari, S., Cecatiello, V., Soffientini, P., Pasqualato, S., and Polo, S. (2013) Structure of a ubiquitin-loaded HECT ligase reveals the molecular basis for catalytic priming. *Nat. Struct. Mol. Biol.* **20,** 696–701 CrossRef Medline
20. Mortensen, F., Schneider, D., Barbic, T., Sladewska-Marquardt, A., Kühnle, S., Marx, A., and Scheffner, M. (2015) Role of ubiquitin and the HPV E6 oncoprotein in E6AP-mediated ubiquitination. *Proc. Natl. Acad. Sci. U.S.A.* **112,** 9872–9877 CrossRef Medline
21. French, M. E., Klosowiak, J. L., Aslanian, A., Reed, S. I., Yates, J. R., 3rd, and Hunter, T. (2017) Mechanism of ubiquitin chain synthesis employed by a HECT domain ubiquitin ligase. *J. Biol. Chem.* **292,** 10398–10413 CrossRef Medline
22. Ronchi, V. P., Kim, E. D., Summa, C. M., Klein, J. M., and Haas, A. L. (2017) *In silico* modeling of the cryptic E2~ubiquitin-binding site of E6-associated protein (E6AP)/UBE3A reveals the mechanism of polyubiquitin chain assembly. *J. Biol. Chem.* **292,** 18006–18023 CrossRef Medline
23. Nuber, U., Schwarz, S. E., and Scheffner, M. (1998) The ubiquitin-protein ligase E6-associated protein (E6-AP) serves as its own substrate. *Eur. J. Biochem.* **254,** 643–649 CrossRef Medline

24. Kao, W. H., Beaudenon, S. L., Talis, A. L., Huibregtse, J. M., and Howley, P. M. (2000) Human papillomavirus type 16 E6 induces self-ubiquitination of the E6AP ubiquitin-protein ligase. *J. Virol.* **74,** 6408–6417 CrossRef Medline
25. Beaudenon, S., Dastur, A., and Huibregtse, J. M. (2005) Expression and assay of HECT domain ligases. *Methods Enzymol.* **398,** 112–125 CrossRef Medline
26. Brzovic, P. S., Lissounov, A., Christensen, D. E., Hoyt, D. W., and Klevit, R. E. (2006) A UbcH5/ubiquitin noncovalent complex is required for processive BRCA1-directed ubiquitination. *Mol. Cell* **21,** 873–880 CrossRef Medline
27. Sakata, E., Satoh, T., Yamamoto, S., Yamaguchi, Y., Yagi-Utsumi, M., Kurimoto, E., Tanaka, K., Wakatsuki, S., and Kato, K. (2010) Crystal structure of UbcH5b~ubiquitin intermediate: insight into the formation of the self-assembled E2~Ub conjugates. *Structure* **18,** 138–147 CrossRef Medline
28. Eletr, Z. M., and Kuhlman, B. (2007) Sequence determinants of E2-E6AP binding affinity and specificity. *J. Mol. Biol.* **369,** 419–428 CrossRef Medline
29. Huang, L., Kinnucan, E., Wang, G., Beaudenon, S., Howley, P. M., Huibregtse, J. M., and Pavletich, N. P. (1999) Structure of an E6AP-UbcH7 complex: insights into ubiquitination by the E2-E3 enzyme cascade. *Science* **286,** 1321–1326 CrossRef Medline
30. Nuber, U., and Scheffner, M. (1999) Identification of determinants in E2 ubiquitin-conjugating enzymes required for hect E3 ubiquitin-protein ligase interaction. *J. Biol. Chem.* **274,** 7576–7582 CrossRef Medline
31. Kamadurai, H. B., Souphron, J., Scott, D. C., Duda, D. M., Miller, D. J., Stringer, D., Piper, R. C., and Schulman, B. A. (2009) Insights into ubiquitin transfer cascades from a structure of a UbcH5B~ubiquitin-HECT^{NEDD4L} complex. *Mol. Cell* **36,** 1095–1102 CrossRef Medline
32. Kim, H. T., Kim, K. P., Lledias, F., Kisselev, A. F., Scaglione, K. M., Skowyra, D., Gygi, S. P., and Goldberg, A. L. (2007) Certain pairs of ubiquitin-conjugating enzymes (E2s) and ubiquitin-protein ligases (E3s) synthesize nondegradable forked ubiquitin chains containing all possible isopeptide linkages. *J. Biol. Chem.* **282,** 17375–17386 CrossRef Medline
33. Hershko, A., and Heller, H. (1985) Occurrence of a polyubiquitin structure in ubiquitin-protein conjugates. *Biochem. Biophys. Res. Commun.* **128,** 1079–1086 CrossRef Medline
34. Tsuchiya, H., Tanaka, K., and Saeki, Y. (2013) The parallel reaction monitoring method contributes to a highly sensitive polyubiquitin chain quantification. *Biochem. Biophys. Res. Commun.* **436,** 223–229 CrossRef Medline
35. Masuda, Y., Kanao, R., Kawai, H., Kukimoto, I., and Masutani, C. (2019) Preferential digestion of PCNA-ubiquitin and p53-ubiquitin linkages by USP7 to remove polyubiquitin chains from substrates. *J. Biol. Chem.* **294,** 4177–4187 CrossRef Medline
36. Camus, S., Higgins, M., Lane, D. P., and Lain, S. (2003) Differences in the ubiquitination of p53 by Mdm2 and the HPV protein E6. *FEBS Lett.* **536,** 220–224 CrossRef Medline
37. Ronchi, V. P., Klein, J. M., Edwards, D. J., and Haas, A. L. (2014) The active form of E6-associated protein (E6AP)/UBE3A ubiquitin ligase is an oligomer. *J. Biol. Chem.* **289,** 1033–1048 CrossRef Medline
38. García-Alai, M. M., Dantur, K. I., Smal, C., Pietrasanta, L., and de Prat-Gay, G. (2007) High-risk HPV E6 oncoproteins assemble into large oligomers that allow localization of endogenous species in prototypic HPV-transformed cell lines. *Biochemistry* **46,** 341–349 CrossRef Medline
39. Zanier, K., Ruhlmann, C., Melin, F., Masson, M., Ould M'hamed Ould Sidi, A., Bernard, X., Fischer, B., Brino, L., Ristriani, T., Rybin, V., Baltzinger, M., Vande Pol, S., Hellwig, P., Schultz, P., and Travé, G. (2010) E6 proteins from diverse papillomaviruses self-associate both *in vitro* and *in vivo*. *J. Mol. Biol.* **396,** 90–104 CrossRef Medline
40. Degenkolbe, R., Gilligan, P., Gupta, S., and Bernard, H. U. (2003) Chelating agents stabilize the monomeric state of the zinc binding human papillomavirus 16 E6 oncoprotein. *Biochemistry* **42,** 3868–3873 CrossRef Medline
41. Zanier, K., ould M'hamed ould Sidi, A., Boulade-Ladame, C., Rybin, V., Chappelle, A., Atkinson, A., Kieffer, B., and Travé, G. (2012) Solution structure analysis of the HPV16 E6 oncoprotein reveals a self-association mechanism required for E6-mediated degradation of p53. *Structure* **20,** 604–617 CrossRef Medline
42. Ronchi, V. P., Klein, J. M., and Haas, A. L. (2013) E6AP/UBE3A ubiquitin ligase harbors two E2~ubiquitin binding sites. *J. Biol. Chem.* **288,** 10349–10360 CrossRef Medline
43. Kumar, S., Kao, W. H., and Howley, P. M. (1997) Physical interaction between specific E2 and Hect E3 enzymes determines functional cooperativity. *J. Biol. Chem.* **272,** 13548–13554 CrossRef Medline
44. Schwarz, S. E., Rosa, J. L., and Scheffner, M. (1998) Characterization of human hect domain family members and their interaction with UbcH5 and UbcH7. *J. Biol. Chem.* **273,** 12148–12154 CrossRef Medline
45. Nuber, U., Schwarz, S., Kaiser, P., Schneider, R., and Scheffner, M. (1996) Cloning of human ubiquitin-conjugating enzymes UbcH6 and UbcH7 (E2-F1) and characterization of their interaction with E6-AP and RSP5. *J. Biol. Chem.* **271,** 2795–2800 CrossRef Medline
46. Martinez-Zapien, D., Ruiz, F. X., Poirson, J., Mitschler, A., Ramirez, J., Forster, A., Cousido-Siah, A., Masson, M., Vande Pol, S., Podjarny, A., Travé, G., and Zanier, K. (2016) Structure of the E6/E6AP/p53 complex required for HPV-mediated degradation of p53. *Nature* **529,** 541–545 CrossRef Medline
47. Lu, Y., Lee, B. H., King, R. W., Finley, D., and Kirschner, M. W. (2015) Substrate degradation by the proteasome: a single-molecule kinetic analysis. *Science* **348,** 1250834 CrossRef Medline
48. Nakagawa, S., Watanabe, S., Yoshikawa, H., Taketani, Y., Yoshiike, K., and Kanda, T. (1995) Mutational analysis of human papillomavirus type 16 E6 protein: transforming function for human cells and degradation of p53 *in vitro*. *Virology* **212,** 535–542 CrossRef Medline
49. Masuda, Y., Suzuki, M., Piao, J., Gu, Y., Tsurimoto, T., and Kamiya, K. (2007) Dynamics of human replication factors in the elongation phase of DNA replication. *Nucleic Acids Res.* **35,** 6904–6916 CrossRef Medline
50. Masuda, Y., Piao, J., and Kamiya, K. (2010) DNA replication-coupled PCNA mono-ubiquitination and polymerase switching in a human *in vitro* system. *J. Mol. Biol.* **396,** 487–500 CrossRef Medline
51. Gu, J., Kawai, H., Wiederschain, D., and Yuan, Z. M. (2001) Mechanism of functional inactivation of a Li-Fraumeni syndrome p53 that has a mutation outside of the DNA-binding domain. *Cancer Res.* **61,** 1741–1746 Medline
52. Katz, C., Low-Calle, A. M., Choe, J. H., Laptenko, O., Tong, D., Joseph-Chowdhury, J. N., Garofalo, F., Zhu, Y., Friedler, A., and Prives, C. (2018) Wild-type and cancer-related p53 proteins are preferentially degraded by MDM2 as dimers rather than tetramers. *Genes Dev.* **32,** 430–447 CrossRef Medline